NK cells shape the clonal evolution of B-ALL cells by IFN-γ production

Michelle C. Buri[1], Mohamed R. Shoeb[1], Aleksandr Bykov[1], Peter Repiscak[1], Hayeon Baik[1], Alma Dupanovic[1], Faith O. David[1], Boris Kovacic[1], Faith Hall-Glenn[1], Jos Urbanus[2], Lisa Sippl[1], Susanne Stofner[1], Dominik Emminger[1], Jason Cosgrove[3], Manfred Lehner[1], Leïla Perié[3], Ton N. Schumacher[2,4], Dagmar Gotthardt[5], Florian Halbritter[1], Eva M. Putz[1, #]

[1] St. Anna Children's Cancer Research Institute (CCRI), Vienna, Austria

[2]Division of Molecular Oncology & Immunology, Oncode Institute, Netherlands Cancer Institute, Amsterdam, The Netherlands

[3] Institut Curie, Université PSL, Sorbonne Université, CNRS UMR168, Laboratoire Physico Chimie Curie, Paris, France

[4] Department of Hematology, Leiden University Medical Center, Leiden, The Netherlands.

[5] Institute of Pharmacology, University of Veterinary Medicine Vienna, Vienna, Austria

[#] Correspondence to eva.putz@ccri.at

Word count: 4652 (Introduction, Results, Discussion)

Number of figures: 5

Number of supplementary figures: 6

Number of supplementary tables: 4

Keywords: cancer immunoediting, natural killer cells, tumour evolution, cytotoxicity, effector function, interferon-γ, perforin, Ly6A, PLAAT3

Abstract (253 words)

The term cancer immunoediting describes the dual role by which the immune system can both suppress and promote tumour growth and is divided into three phases: elimination, equilibrium and escape. While the importance of $CD8^+$ T cells in all three phases of cancer immunoediting is well-established, the role of NK cells has mainly been attributed to the elimination phase. Here we show that NK cells play a prominent role in all three phases of cancer immunoediting. Extended co-culturing of DNA barcoded mouse BCR/ABL^{p185+} B acute lymphoblastic leukaemia cells with NK cells allowed for a quantitative measure of NK cell-mediated immunoediting *in vitro*. Whereas most tumour cell clones were efficiently eliminated by NK cells, a certain fraction of tumour cells harboured an intrinsic resistance. Furthermore, DNA barcoding revealed tumour cell clones with secondary resistance, which stochastically acquiring resistance to NK cells. We found that the production of interferon-γ (IFN-γ) rather than direct cytotoxicity by NK cells, led to the emergence of highly resistant tumour cells. Besides the well-known upregulation of components involved in major histocompatibility complex I surface expression, we also found novel genes that had not previously been linked to NK cell resistance in leukaemic cells, such as *Ly6a* and *Plaat3*. Our results demonstrate that tumour cells are actively edited during the equilibrium phase and use different avenues to escape NK cell-mediated eradication. Our findings provide a starting point to develop novel therapeutic approaches to treat tumours that have successfully evaded from NK cell surveillance and to convert them into a controllable disease.

Main/Introduction

Cancer immunoediting refers to the dynamic interaction between immune cells and cancer cells during tumour development[1]. The immune system can have both tumour-promoting and tumour-suppressive effects. This process occurs in three phases: elimination, equilibrium, and escape. In the elimination phase, adaptive and innate immune cells, particularly cytotoxic T and NK cells, recognise and eliminate cancer cells. The equilibrium phase involves the coexistence of tumour cells and the immune system, leading to sculpting of the tumour under constant immune pressure, ultimately resulting in immune escape[2].

NK cells are innate lymphoid cells with the ability of recognising and eliminating damaged, stressed, and infected cells including cancer cells[3]. NK cell activation relies on a balance of activating and inhibitory signals from receptors on their surface during the interaction with potential target cells. On one hand, activated NK cells can kill target cells through exocytosis of cytotoxic granules containing perforin and granzymes[4], induction of death receptor-mediated apoptosis[5] or antibody-dependent cellular cytotoxicity (ADCC) via their FcγRIIIA (CD16) receptor[6]. On the other hand, NK cells secrete cytokines such as interferon-γ (IFN-γ), which activate other immune cells in their vicinity[7,8]. In the context of cancer immunoediting, NK cells play a crucial role in eliminating tumour cells during the elimination phase and limiting the metastatic spread of tumour cells after immune evasion. NK cells spare healthy tissue and present a safe treatment option with reduced risk of causing adverse effect such as cytokine release syndrome or graft versus host disease[9]. As a result, there is growing interest in using NK cells for immunotherapies, which will benefit from a better understanding of how tumour cells evade NK cell attacks to effectively target their Achilles heel. However, most studies to date have focused on the interaction between human NK cells and tumour cell lines obtained from patients[10–14]. These tumour cells have already successfully evaded from the patient´s immune system and may thus not represent suitable models to study immunoediting.

Here, we used a model based on non-edited NK cell-naïve mouse BCR/ABL^{p185+} B cell acute lymphoblastic leukaemia (B-ALL) cells to investigate the primary interaction of tumour cells

with NK cells. This model involves a long-term co-culture of tumour cells and primary NK cells. By analysing the NK cell-resistant tumour cells that emerge during the co-culture, we investigated molecular changes using RNA sequencing (RNA-seq) and assay for transposase-accessible chromatin sequencing (ATAC-seq). The results indicate that the transcriptomic changes in the resistant tumour cells are mainly due to IFN-γ secretion by NK cells, which upregulates genes like lymphocyte antigen 6 complex, locus A (*Ly6a*) and phospholipase A and acyltransferase 3 (*Plaat3*). This study identified Ly6A and PLAAT3 as novel potential drivers of NK cell-mediated immune evasion of leukaemia. Moreover, we established a model to quantify NK cell effector functions and their ability to edit DNA barcoded tumour cells. Cellular DNA barcoding stably introduces unique inheritable DNA sequences that allows tracking of individual cell clones and their fates within a heterogeneous cell population[15–17]. Thereby, we observed that, while some tumour cells were inherently resistant or sensitive to NK cells, a few tumour cells were edited by NK cells to become resistant. In summary, this study shows that NK cells play an important role in all three phases of cancer immunoediting and contribute to the active sculpting of tumour cell clones, ultimately driving tumour evasion.

Results

Quantitative measure of NK effector functions

As a model to study NK cell evasion of leukaemic tumour cells we established a long-term *in vitro* co-culture system using IL-2-activated primary mouse NK cells co-incubated with NK-naïve DNA barcoded B-ALL cell lines for up to 20 days (**Figure 1A**). We generated several independent B-ALL cell lines from the bone marrow of wild-type (n=10) and major histocompatibility complex 1 (MHC-1)-deficient *B2m*$^{-/-}$ mice (n=10) and characterised their NK receptor ligand surface expression and their susceptibility towards NK cell-mediated eradication at an effector-to-target (E:T) ratio of 10:1. Summarizing this data by unsupervised hierarchical clustering (**Figure 1B**) highlighted the two wild-type cell lines #13 and #15 which

showed the highest susceptibility towards NK cells and expressed enhanced levels of activating NKG2D-ligand Rae1 and lower levels of inhibitory ligands (e.g. classical and non-classical MHC-1 proteins H2-K^b, H2-D^b, Qa-1^b and Qa-2). *B2m*-deficient B-ALL cell lines showed a higher susceptibility towards NK cells according to the recognition of missing self[18] (see **Figure S1A** for full characterisation). To allow for a systematic quantification of NK cell effector functions, a DNA barcode library was introduced into the wild-type B-ALL cell lines #13 and #15 (n=2 each) and the *B2m*$^{-/-}$ (n=1) cell line #23 to track individual tumour cell clones over time. For this purpose, a new lentiviral barcode library (LG2.1, containing 52,645 barcodes in the reference list) was generated consisting of 21 random nucleotides positioned downstream of a green fluorescent protein (*GFP*) gene (**Figures S1B-E**). The lentiviral library was introduced into the B-ALL cell lines at a low multiplicity of infection (MOI) to ensure the integration of a single barcode per cell as previously described[19,20] (**Figure 1C**). To enrich for barcoded cells, GFP$^+$ cells were FACS sorted shortly after transduction and before the long-term co-culture with IL-2-activated NK cells. The barcode diversity of the resulting four cell lines called A and B (derived from #13), C and D (derived from #15) was determined by site-specific PCR amplification and next generation sequencing (**Figure 1D**). The barcoded cells were co-incubated with IL-2-activated NK cells at an E:T ratio of 1:1. After 4 and 14 days, GFP$^+$ tumour cells were FACS purified and fresh NK cells were replenished to re-challenge the tumour cells. Throughout the experiment, the absolute number of GFP$^+$ tumour cells was determined by regular flow cytometric analysis (**Figure 1E**). While the tumour cells initially showed significantly slower proliferation in the presence of NK cells during the first two rounds of co-culture, this difference became marginal in the third round. Twenty-five days after the start of co-culture, we performed a classical 4-hour cytotoxicity assay with tumour cells that had been co-cultured with NK cells for 20 days versus NK-naïve tumour cells. As shown in **Figure 1F**, extended co-culture of NK and leukaemic cells induced resistance towards NK cell-mediated killing and led to tumour evasion *in vitro*.

NK cell-mediated editing of leukaemic cells

There are four conceivable fates of B-ALL tumour cell clones upon long-term co-culture with NK cells: The abundance of one clone could be lower ("eliminated"), higher ("primary resistant"), unchanged ("static") or highly variable ("secondary resistant") (**Figure 2A**). After bulk DNA sequencing of the barcodes, we designed a decision tree to discriminate these four categories algorithmically (**Figure 2B**). Primary resistance, also known as intrinsic resistance[21], is defined as *a priori* resistance towards therapy. In our study, primary resistance was characterised by a reproducible and significant accumulation despite the presence of NK cells in co-culture. In comparison, secondary resistance describes the phenomenon of acquired resistance, represented by a situation in which a tumour can initially respond effectively to therapy but relapse or progress after treatment[22]. We hypothesised that acquired secondary resistance was not a tumour-intrinsic property but acquired only in a subfraction of sibling cells and would be observed in isolated wells (**Figure 2A**). Indeed, clustering the DNA barcoded leukaemic cells according to our four pre-defined categories (**Figure 2C, S2A** for summary data), showed that the majority of leukaemic cell clones was efficiently eliminated (58.5±1.4% considering n=2-3 independent experiments comprising n=2-4 B-ALL cell lines, mean±SEM). Only a smaller number of leukaemic cell clones seemed to have an NK cell resistant phenotype (14.3±1.3%). About 23.9±1.4% of the B-ALL cell clones remained static despite the presence of NK cells. As hypothesised, we also observed B-ALL cell clones that showed secondary resistance, characterised by the presence of the cell clone in only 1/3 replicate wells (3.3±0.8%, **Figure 2D**). To be able to draw conclusions about the pre-existing fate of the tumour cell clones, we compared two independent experiments with the same barcoded cell lines. As shown in **Figures 2E and S2B**, the cell clones attributed to the clusters primary resistant and eliminated were found to have the same fate in both experiments. In contrast, the pool of secondary resistant tumour cell clones was distinctive for independent experiments. In summary, our data suggest that, whereas primary resistant and eliminated cells harbour tumour-intrinsic properties *a priori* that determine their destiny, the fate of secondary resistant tumour cell clones is stochastic.

This underscores our hypothesis that secondary resistant tumour cells acquire their resistant phenotype during NK co-culture. Our data clearly show that apart from direct killing, NK cells participate in immunoediting by actively shaping the tumourigenicity of individual tumour cells.

Molecular changes observed in NK cell resistant B-ALL cells

To identify novel drivers of NK cell resistance we investigated the changes in the transcriptomic and chromatin accessibility profiles of the NK cell-resistant B-ALL cell lines generated during the long term *in vitro* co-culture. To this end, we performed RNA (**Figures 3A-D, S3A-E**) and ATAC sequencing (**Figures 3E-F, S3F-H**) and compared NK co-cultured to NK naïve tumour cells. The transcriptomic analysis showed a significant upregulation of genes with a well-known link to NK cell immune evasion such as *Lgals3bp*[23] and several components of the MHC-I machinery (e.g., *Stat1*, *B2m*, *Tap1* and *H2-K1*[24]). Additionally, this analysis revealed a novel set of genes, which may include potential drivers of NK cell resistance, such as *Ly6a* and *Plaat3* (**Figure 3A, Figures S3C-E**). The functional enrichment analysis showed that the main biological process associated with the differentially expressed genes was the response to IFN-γ (e.g., *Stat1*, *Irf1*, *Ccl5* and *Cd74*), which is produced by activated NK cells in co-culture (**Figure 3B**). After integrating the results from the four barcoded cell lines A-D, we observed that many differentially expressed genes upon NK cell co-culture were cell line specific (up: A/B=193 and C/D=99, down: A/B: 211 and C/D=63). However, a total of 129 genes were up- and 27 were downregulated in all four cell lines and may be universally associated with or driving NK cell escape (**Figure 3C**). The top-30 differentially regulated genes are depicted in the heat map in **Figure 3D**. In line, the ATAC sequencing results showed the opening of chromatin at the promoters of classical interferon-inducible genes (e.g., *Iigp1*, *Ifi27*, *Mx1*), as well as *Ly6a* and *Plaat3*, genes previously observed in the RNA sequencing dataset (**Figure 3E, S3H**). We considered overlapping differentially accessible regions (DARs) in cell lines A/B and C/D as the most robust ones (**Figure 3F**). Integration of RNA and ATAC sequencing data by comparing the differentially expressed genes and accessible regions in cell lines A/B showed a significant intersection

(37 genes up/open, 16 genes down/closed). Interestingly, the two highly upregulated genes *Ly6a* and *Plaat3* in the transcriptomic analysis were also present in this strictly filtered data set (**Figure 3G**). The quantification of differential transcription factor (TF) activity by integrating the RNA- and ATAC-seq data sets revealed key TFs involved in NK cell resistance. We classified TFs as activators (NF2L1, SMRC1, JUN, IRF1 and IRF9) or repressors (RXRB, JUND), based on the expression of the corresponding TF and accessibility of predicted binding sites[25]. STAT1 expression was clearly upregulated but appears to have activating and repressive functions and is therefore classified as undetermined (**Figure 3H**). A closer look at the two top hits *Ly6a* and *Plaat3* showed that both have multiple predicted binding sites for STAT1, IRF1 and IRF9 based on the occurrence of DNA sequence motifs in the vicinity of accessible chromatin (**Figure 3I**). In summary, multiomics analyses revealed that the B-ALL cells, which were not *a priori* sensitive and eliminated by NK cells, showed a highly NK cell-resistant phenotype characterised by a strong IFN-γ signature.

IFN-γ as major driver of cancer immunoediting

The two main functions of NK cells are the direct lysis of tumour cells and the production of pro-apoptotic and -inflammatory cytokines, most importantly IFN-γ. Thus, we aimed to discriminate the relative contributions of killing and cytokine production to cancer immunoediting. To determine the share of direct cytotoxicity, the long-term co-culture experiment was performed with NK cells proficient (WT) or deficient for the pore-forming protein perforin (*Prf1*$^{-/-}$). This deficiency renders them unable to directly kill their target cells[26]. In parallel, B-ALL cells were treated continuously with recombinant IFN-γ. As described above, the growth of GFP^{+} tumour cells was measured by flow cytometry during the experiment. On day 4 and 14, GFP^{+} tumour cells were sorted and co-cultured with freshly prepared WT NK or *Prf1*$^{-/-}$ NK cells or treated continuously with IFN-γ. As previously observed, B-ALL cells co-cultured with WT NK cells showed an initial susceptibility during the first 14 days and developed an NK resistance thereafter (**Figure 4A**). As expected, *B2m*$^{-/-}$ B-ALL tumour cells did not survive the co-culture with WT NK cells (**Figure S5A**). In contrast,

B-ALL and *B2m*$^{-/-}$ B-ALL cells co-cultured with *Prf1*$^{-/-}$ NK cells or treated with IFN-γ showed a minor but consistent growth inhibition compared to untreated B-ALL cells. This showed that NK cell-derived cytokines, and in particular IFN-γ, had a direct effect on the growth of B-ALL cells (**Figures 4A and S5A**). However, the cytotoxicity assay performed on day 28 after treatment start showed that B-ALL cells continuously treated with IFN-γ were most resistant to WT NK cells (**Figures 4B and S5B**).

On day 14, the B-ALL cells were further analysed for their clonal diversity and transcriptomic profiles. In line with our previous experiments, the barcode diversity of the B-ALL + WT NK cell condition was markedly decreased (**Figure 4C**). The tumour cells co-cultured with *Prf1*$^{-/-}$ NK cells or treated with IFN-γ showed a milder decrease of tumour cell diversity (**Figure 4C**). Interestingly, we observed a strong overlap of eliminated and primary resistant tumour cell clones in all three treatment groups, WT NK, *Prf1*$^{-/-}$ NK cell and IFN-γ, suggesting that these cell clones were intrinsically susceptible or resistant to IFN-γ-mediated apoptosis (**Figure 4D**). Apart from the primary resistant tumour cells, we detected cell clones, which acquired resistance due to the NK co-culture or IFN-γ treatment (resistant (2nd)). Strikingly, the number of secondary resistant tumour cell clones was the largest in the B-ALL + WT NK cell condition (n=56 versus 15 and 12 cell clones in B-ALL + *Prf1*$^{-/-}$ NK or IFN-γ, respectively). These findings led us to conclude that NK cells exert an immunological pressure on tumour cells, which is partly independent of IFN-γ production (**Figures 4D&E**). To define the molecular changes driving NK cell resistance in B-ALL cells upon co-culture with WT or *Prf1*$^{-/-}$ NK cells or treatment with IFN-γ, we compared the transcriptomic profiles of all conditions on day 14 after start of treatment. As expected, IFN-γ treatment induced a large number of genes, which overlapped with some of the most significant hits of WT NK and *Prf1*$^{-/-}$ NK cells (23 up- and 10 downregulated genes), such as *Ly6a* and *Plaat3*. We reasoned that changes in gene expression unique for the WT NK cell condition were due to the direct NK cell killing. For instance, we identified an upregulation of *Bnip3*, which was recognised as important player in immune evasion from NK cells before[27]. Additionally, *Aldoa* and *Pgk1* were found to be upregulated, both of which are involved in glycolysis and associated with worse prognosis

in pancreatic, cervical and breast cancer[28,29] (**Figures 4F&G and S4**). In conclusion, IFN-γ on the one hand contributed to the selective pressure of NK cells, but on the other hand prolonged IFN-γ exposure led to the dominance of tumour cells that were less sensitive to NK cell attack.

Role of Ly6a and Plaat3 in tumour evasion

NK cell resistance in B-ALL cells was associated with altered expression of well-known and novel genes involved in cancer immunoediting. We demonstrated in multiple experiments that the mouse surface stem cell marker *Ly6a* and *Plaat3* belong to the most significantly upregulated genes in NK resistant B-ALL cell lines. Therefore, we decided to follow up on these two genes and unravel their role in immune evasion. We performed the co-culture experiment as described in **Figure 4** and analysed the B-ALL cells on day 14 by mass spectrometry to confirm the upregulation of Ly6A and PLAAT3 on the protein level. Indeed, Ly6A protein expression was increased after WT or *Prf1*$^{-/-}$ KO NK cell co-culture and even more upon IFN-γ treatment (**Figure 5A**). After deletion of *Ly6a* in B-ALL cells by CRISPR/Cas9 genome editing, the surface protein expression was undetectable in flow cytometry (**Figure 5B**). Ly6A deficiency had no impact on B-ALL cell proliferation or survival (**Figures S6A&B**). Although IFN-γ production by NK cells as well as surface ligand expression relevant for NK cell interaction was unchanged (**Figures S6C&D**), *Ly6a* KO clones were more susceptible to NK cells compared to WT clones in cytotoxicity assays (**Figure 5C**). This result clearly shows that Ly6A plays an important role in NK immune evasion of mouse B-ALL cells.

Likewise, we generated *Plaat3* KO B-ALL clones and verified the lack of *Plaat3* mRNA by qPCR (**Figure 5E**). *Plaat3* KO cells did not show any difference in proliferation and viability, IFN-γ production by NK cells and NK receptor ligand expression (**Figures S6E-H**). In contrast to *Ly6a*, loss of *Plaat3* did not have any impact on direct NK cell-mediated killing of mouse B-ALL cells (**Figure 5F**). To test the relevance of the human orthologue *PLAAT3* in leukaemia, we analysed the *PLAAT3* expression of patients with various leukaemia subtypes. We observed that an increased *PLAAT3* expression correlated with worse overall

survival in diffuse large B cell lymphoma (DLBCL), acute myeloid leukaemia (AML) and acute lymphoblastic leukaemia (ALL) patients (**Figures 5G-I**). In line, the oncogenic function of PLAAT3 was supported by previous studies in osteosarcoma and non-small cell lung carcinoma[30–32].

In summary, our functional analysis of Ly6A and PLAAT3 showed that their expression is upregulated by IFN-γ and Ly6A was identified as a novel driver of tumour evasion from NK cells. Although PLAAT3 did not lead to NK cell resistance in our mouse model, its increased expression in leukaemic cells correlated with poor disease outcome in patients.

Discussion

NK cells represent a potent arm of the immune system, tasked with eliminating anomalous cells. Nonetheless, they can fail controlling cancer cells which successfully evaded from the immune surveillance. The presented study aimed to elucidate the evasion mechanisms employed by tumour cells to escape NK cells during initial encounter and extends earlier efforts using patient derived tumour cell lines[10,11,33–37]. Notably, patient-derived cell lines have already undergone the cancer immunoediting process and thus have acquired strategies to evade the immune system. On the contrary, our study is based on heterogeneous, non-edited and immune-naïve mouse BCR/ABL^{p185+} B-ALL tumour cell lines. This unique model enables to explore the primary interplay between tumour cells and the immune system. Furthermore, the B-ALL tumour cells have been DNA barcoded, a technique that allows for the quantification of tumour cell clonal dynamics, which can help to better understand the mechanisms of NK cell effector function. To the best of our knowledge, this particular aspect has not been demonstrated in previous studies.

We established an *in vitro* model, whereby mouse NK and DNA barcoded B-ALL cells were co-cultured for several days. Transcriptome analysis, assessment of chromatin accessibility and evaluation of clonal evolution were performed at two time points during the experiment. DNA barcoding allowed the determination of tumour cell fate during the co-culture and revealed that most tumour cell clones possessed inherent sensitivity or resistance to NK

cells. This technique has already been used by many others to quantify tumour cell susceptibility towards immune cells, drug- or antibody-based immunotherapies[38–41]. Similar to our research, these studies observed that the majority of tumour cells are predestined for distinct sensitivity or resistant fates upon treatment. For instance, Baldwin et al. found pre-existing resistant clones which were positively selected after combined anti-PD1 and anti-CTLA4 therapy in mouse mammary cancer and their gene expression signature correlated with worse survival in patients[40]. Beyond those two fundamental fates of life and death, our study highlighted tumour cell clones, which acquired resistance in the presence of NK cells. Secondary resistance was only observed in a small subset of tumour cell clones, which showed NK cell resistance in only one of three replicate wells on day 14. Similarly, using DNA barcoding to investigate the clonal evolution of drug-treated lung cancer cells, Acar *et al.* recently described the emergence of "*de novo* resistant lineages" in one replicate only[38]. Interestingly, we found that secondary resistant tumour cells were highly distinctive for each independently performed experiment, suggesting that a stochastic event causes the resistance. This demonstrates that NK cells can shape tumour cells and contribute to immunoediting of tumour cell clones. However, due to the necessity of expanding the barcoded cell lines before the experiments (to ensure reproducible representation of all barcodes in every well), we cannot formally exclude the possibility of pre-existing heterogeneity within a cell clone. Furthermore, the LG2.1 barcode library used here was found to be incompatible with single-cell RNA sequencing, as the barcode sequence is located approximately 900 bps upstream of the polyA tail and could not be detected by direct sequencing. It would certainly be highly interesting to delve deeper into secondary resistance mechanisms and to compare the transcriptomic profiles of primary and secondary resistant tumour cell clones in the future[42,43].

We show that NK cells exert immunological pressure on tumour cells, which eventually escape and become refractory to NK cell killing. Previously described NK cell tumour evasion mechanisms include the upregulation of proteins involved in antigen presentation and MHC-I and -II molecules[44,45], the loss or shedding of NKG2D ligands such as MHC class I chain-

related molecule A and B (MICA/B)[46] and secretion of TGF-β and IL-10[47]. Notably, we here describe *Ly6a* and *Plaat3* overexpression as emerging novel drivers of tumour evasion. Ly6A, also called stem cell antigen-1 (Sca-1), is an 18-kDa mouse glycosyl phosphatidylinositol-anchored cell surface protein. It plays an important role in haematopoietic progenitor/stem cell lineage fate, brain blood barrier transport and cancer stem cell biology[48–51]. Ly6A was shown to be upregulated in gastric cancer stem cells and mammary tumours induced by Wnt/β-Catenin signalling and TGF-β deregulation. This promoted cell migration *in vitro,* increased tumourigenicity and resistance to chemotherapy *in vivo*[51–54]. The human orthologue for *Ly6a* has been under debate. Two independent groups recently suggested that the human orthologue *LY6A*/*LY6S* is located in region 8q24.3 of the human genome and is upregulated upon IFN-γ treatment and in pituitary tumours[55,56]. Interestingly, Hossiny *et al.* showed that LY6E and LY6K, which had been discussed previously as the human orthologues of *Ly6a*, promote breast cancer *in vivo* and drive drug sensitivity and epithelial-to-mesenchymal transition (EMT). Moreover, they observed that LY6E/LY6K are required for TGF-β signalling and facilitate immune evasion by upregulating PD-L1 on cancer cells, by recruiting T-regulatory cells and dampening NK cell activation[57]. Our results support the observed oncogenic and immune suppressive properties of Ly6A showing that it is highly upregulated after NK cell co-culture and inducible by IFN-γ. Although the exact mechanism remains unknown, the sensitivity towards NK cells increased significantly upon *Ly6a* gene deletion. Our results support the notion that immunoedited and thus more aggressive tumour cells may harbour cancer stem cell (CSC) features. CSCs are considered responsible for metastasis and therapy resistance, as they are characterised by deregulated differentiation, self-renewal, drug resistance, and amongst others evasion of immunosurveillance. Unlike other immune cells, NK cells are believed to show direct cytotoxicity against CSCs[58]. On the other hand, as CSCs frequently upregulate classical and non-classical MHC-I molecules while losing NK cell activating ligands, it is still a matter of debate if and how NK cells are able to detect and kill CSCs[58,59].

In our multiomics analysis, we showed that *Plaat3* is significantly upregulated in B-ALL cells upon co-culture with WT NK cells, *Prf1*$^{-/-}$ NK cells and treatment with IFN-γ. There was no difference in direct NK cell-mediated killing upon *Plaat3* gene deletion in our mouse B-ALL model, probably due to its relatively low expression under basal conditions. However, it is noteworthy that increased expression of *PLAAT3* in patients with DLBCL, AML and ALL correlates with worse overall survival, which suggests that *PLAAT3* plays a role in leukaemia patients. PLAAT3 belongs to the phospholipase A2 (Pla2) family, which is primarily known to catalyse hydrolysis at the sn-2 ester bond and therefore generate free fatty acids and lysophospholipids, such as arachidonic acid[60,61]. PLAAT3 is usually highly expressed in adipose tissue and regulates lipolysis by controlling the amount of arachidonic acid (AA)[62]. AA is involved in the production of prostaglandins mediated by cyclooxygenase-2 (COX-2)[63]. It is thus assumed that the upregulation of PLAAT3 in cancer cells would increase AA levels and thereby boost the COX-2-mediated production of prostaglandins, prostaglandin E2 (PGE_2) amongst others. PGE_2 has potent immunosuppressive and tumour promoting functions. In NK cells, PGE_2 specifically inhibits target cell killing, cytokine production, and chemotactic activity via the prostaglandin E receptor 4 (EP4)[64–68]. *PLAAT3* is a direct transcriptional target of mutant p53[30] and is frequently upregulated in cancer, correlating with metastasis and poor prognosis in human solid tumours[31,32]. This aligns well with our survival analysis in leukaemia patient cohorts. Previous studies revealed that PLAAT3 overexpression increases the proliferation, migration, invasion, survival and colony formation of osteosarcoma cells, leading to bigger tumours when transplanted in NK cell sufficient Nude mice[31]. In our hands, *Plaat3* deletion in B-ALL cells had no effect on the proliferation of the tumour cells, nor did it impact the NK cell-mediated killing or IFN-γ production. Further research is needed to better understand the role of PLAAT3 in leukaemia.

In general, this research underscores the pivotal role of IFN-γ in the acquisition of NK cell resistance and as ultimate driver of immune evasion. In contrast, *in vitro* and *in vivo* gene-editing screens showed that loss of IFN-γ signalling (IFNGR1/2, JAK1/2, etc.) and antigen presentation (B2M, TAP1, etc.) leads to immune evasion from T cells or resistance to

immunotherapies[69–71]. However, downregulation of MHC-I converts the tumour cells to prime NK cell targets. It was thus proposed to treat tumours with an NK cell-based therapy to antagonize immune escape from T cells[35]. In our experiments, tumour cells responded to the NK cell co-culture with an upregulation of many IFN-γ inducible genes, such as MHC-I molecules, thereby inhibiting NK cells and inducing resistance. We sought to uncover the role of IFN-γ by comparing the tumour cells co-cultured with WT NK cells to tumour cells treated with IFN-γ. By using DNA barcoding we were able to quantify the effect of IFN-γ on tumour cells and dissect IFN-γ dependent and independent tumour cell fates. We observed that a major part of NK cell susceptible clones overlapped well with the eliminated clones upon IFN-γ treatment (527 of 795 clones). We thus concluded that IFN-γ plays on one hand a major role in tumour cell elimination and on the other hand enhances NK cell resistance of the remaining tumour cells by upregulating IFN-γ dependent genes, such as genes involved in MHC-I representation, *Ly6a* and *Plaat3*. The pro-apoptotic functions of IFN-γ have been observed previously in diverse tumour types. IFN-γ signalling was recognised to induce apoptosis-related genes such as caspase 3 and caspase 7 mainly via the JAK/STAT1 pathway[72–75]. Although IFN-γ has profound antiproliferative and proapoptotic effects against cancer cells, IFN-γ treatment of cancer patients achieved only minor success probably due to its poor therapeutic index[76]. Additionally, it has been proposed that IFN-γ has a dual role in cancer[77]. Its anti- and protumorigenic activities are dependent on the duration (acute versus chronic), magnitude of IFN-γ signalling and the immune cell composition. A deeper understanding of the multifaceted actions of IFN-γ is needed to provide patients the most promising treatment options.

In conclusion, our work sheds light on the intricate interplay between NK and leukaemic cells during initial encounters. Here we show that tumour cells are actively shaped by NK cells and use different ways to NK cell-mediated eradication. By dissecting evasion mechanisms and identifying potential key genes, this study contributes to unravelling cancer evasion strategies. Further research, especially *in vivo*, is required to delve deeper into the tumour

evasion mechanisms involving Ly6A and PLAAT3. These findings ultimately deepen our understanding of cancer immune evasion.

References:

1. Gubin, M. M. & Vesely, M. D. Cancer Immunoediting in the Era of Immuno-oncology. *Clin. Cancer Res.* **28**, 3917–3928 (2022).
2. Dunn, G. P., Bruce, A. T., Ikeda, H., Old, L. J. & Schreiber, R. D. Cancer immunoediting: from immunosurveillance to tumor escape. *Nat. Immunol.* **3**, 991–998 (2002).
3. Wolf, N. K., Kissiov, D. U. & Raulet, D. H. Roles of natural killer cells in immunity to cancer, and applications to immunotherapy. *Nat. Rev. Immunol.* **23**, 90–105 (2023).
4. Metkar, S. S. *et al.* Cytotoxic Cell Granule-Mediated Apoptosis: Perforin Delivers Granzyme B-Serglycin Complexes into Target Cells without Plasma Membrane Pore Formation. *Immunity* **16**, 417–428 (2002).
5. Prager, I. & Watzl, C. Mechanisms of natural killer cell-mediated cellular cytotoxicity. *J. Leukoc. Biol.* **105**, 1319–1329 (2019).
6. Wang, W. NK cell-mediated antibody-dependent cellular cytotoxicity in cancer immunotherapy. *Front. Immunol.* **6**, (2015).
7. Huntington, N. D., Cursons, J. & Rautela, J. The cancer–natural killer cell immunity cycle. *Nat. Rev. Cancer* **20**, 437–454 (2020).
8. Bald, T., Krummel, M. F., Smyth, M. J. & Barry, K. C. The NK cell–cancer cycle: advances and new challenges in NK cell–based immunotherapies. *Nat. Immunol.* **21**, 835–847 (2020).
9. Liu, E. *et al.* Use of CAR-Transduced Natural Killer Cells in CD19-Positive Lymphoid Tumors. *N. Engl. J. Med.* **382**, 545–553 (2020).
10. Bernareggi, D. *et al.* CHMP2A regulates tumor sensitivity to natural killer cell-mediated cytotoxicity. *Nat. Commun.* **13**, 1899 (2022).
11. Chiba, M. *et al.* Genome-wide CRISPR screens identify CD48 defining susceptibility to NK cytotoxicity in peripheral T-cell lymphomas. *Blood* **140**, 1951–1963 (2022).
12. Pech, M. F. *et al.* Systematic identification of cancer cell vulnerabilities to natural killer cell-mediated immune surveillance. *eLife* **8**, e47362 (2019).

13. Sheffer, M. *et al.* Genome-scale screens identify factors regulating tumor cell responses to natural killer cells. *Nat. Genet.* **53**, 1196–1206 (2021).
14. Carré, T. *et al.* Selection of tumor-resistant variants following sustained natural killer cell-mediated immune stress. *Oncol. Rep.* **45**, 582–594 (2021).
15. Naik, S. H., Schumacher, T. N. & Perié, L. Cellular barcoding: A technical appraisal. *Exp. Hematol.* **42**, 598–608 (2014).
16. Eisele, A. S. *et al.* Erythropoietin directly remodels the clonal composition of murine hematopoietic multipotent progenitor cells. *eLife* **11**, e66922 (2020).
17. Marsolier, J. *et al.* H3K27me3 conditions chemotolerance in triple-negative breast cancer. *Nat. Genet.* **54**, 459–468 (2022).
18. Kärre, K., Ljunggren, H. G., Piontek, G. & Kiessling, R. Selective rejection of H–2-deficient lymphoma variants suggests alternative immune defence strategy. *Nature* **319**, 675–678 (1986).
19. Naik, S. H. *et al.* Diverse and heritable lineage imprinting of early haematopoietic progenitors. *Nature* **496**, 229–32 (2013).
20. Eisele, A. S. *et al.* Erythropoietin directly remodels the clonal composition of murine hematopoietic multipotent progenitor cells. *eLife* **11**, e66922 (2022).
21. Bai, R. *et al.* Mechanisms of Cancer Resistance to Immunotherapy. *Front. Oncol.* **10**, 1290 (2020).
22. Sharma, P., Hu-Lieskovan, S., Wargo, J. A. & Ribas, A. Primary, Adaptive, and Acquired Resistance to Cancer Immunotherapy. *Cell* **168**, 707–723 (2017).
23. Capone, E., Iacobelli, S. & Sala, G. Role of galectin 3 binding protein in cancer progression: a potential novel therapeutic target. *J. Transl. Med.* **19**, 405 (2021).
24. Zhou, F. Molecular Mechanisms of IFN-γ to Up-Regulate MHC Class I Antigen Processing and Presentation. *Int. Rev. Immunol.* **28**, 239–260 (2009).
25. Berest, I. *et al.* Quantification of Differential Transcription Factor Activity and Multiomics-Based Classification into Activators and Repressors: diffTF. *Cell Rep.* **29**, 3147-3159.e12 (2019).

26. Kägi, D. *et al.* Cytotoxicity mediated by T cells and natural killer cells is greatly impaired in perforin-deficient mice. *Nature* **369**, 31–37 (1994).
27. Macher-Goeppinger, S. *et al.* Expression and Functional Characterization of the BNIP3 Protein in Renal Cell Carcinomas. *Transl. Oncol.* **10**, 869–875 (2017).
28. Ji, S. *et al.* ALDOA functions as an oncogene in the highly metastatic pancreatic cancer. *Cancer Lett.* **374**, 127–135 (2016).
29. He, Y. *et al.* PGK1-mediated cancer progression and drug resistance. *Am. J. Cancer Res.* **9**, 2280–2302 (2019).
30. Xiong, S. *et al.* Pla2g16 phospholipase mediates gain-of-function activities of mutant p53. *Proc. Natl. Acad. Sci. U. S. A.* **111**, 11145–11150 (2014).
31. Li, L. *et al.* PLA2G16 promotes osteosarcoma metastasis and drug resistance via the MAPK pathway. *Oncotarget* **7**, 18021–18035 (2016).
32. Nazarenko, I. *et al.* H-REV107-1 stimulates growth in non-small cell lung carcinomas via the activation of mitogenic signaling. *Am. J. Pathol.* **169**, 1427–1439 (2006).
33. Pech, M. F. *et al.* Systematic identification of cancer cell vulnerabilities to natural killer cell-mediated immune surveillance. *eLife* **8**, e47362 (2019).
34. Zhuang, X., Veltri, D. P. & Long, E. O. Genome-Wide CRISPR Screen Reveals Cancer Cell Resistance to NK Cells Induced by NK-Derived IFN-γ. *Front. Immunol.* **10**, (2019).
35. Freeman, A. J. *et al.* Natural Killer Cells Suppress T Cell-Associated Tumor Immune Evasion. *Cell Rep.* **28**, 2784-2794.e5 (2019).
36. Sheffer, M. *et al.* Genome-scale screens identify factors regulating tumor cell responses to natural killer cells. *Nat. Genet.* **53**, 1196–1206 (2021).
37. Dubrot, J. *et al.* In vivo CRISPR screens reveal the landscape of immune evasion pathways across cancer. *Nat. Immunol.* **23**, 1495–1506 (2022).
38. Acar, A. *et al.* Exploiting evolutionary steering to induce collateral drug sensitivity in cancer. *Nat. Commun.* **11**, 1923 (2020).
39. Umkehrer, C. *et al.* Isolating live cell clones from barcoded populations using CRISPRa-inducible reporters. *Nat. Biotechnol.* **39**, 174–178 (2021).

40. Baldwin, L. A. *et al.* DNA barcoding reveals ongoing immunoediting of clonal cancer populations during metastatic progression and immunotherapy response. *Nat. Commun.* **13**, 6539 (2022).
41. Goyal, Y. *et al.* Diverse clonal fates emerge upon drug treatment of homogeneous cancer cells. *Nature* **620**, 651–659 (2023).
42. Weinreb, C., Rodriguez-Fraticelli, A., Camargo, F. D. & Klein, A. M. Lineage tracing on transcriptional landscapes links state to fate during differentiation. *Science* **367**, eaaw3381 (2020).
43. Chang, M. T. *et al.* Identifying transcriptional programs underlying cancer drug response with TraCe-seq. *Nat. Biotechnol.* **40**, 86–93 (2022).
44. Ljunggren, H.G. & Kärre, K. In serach of the 'missing self': MHC molecules and NK cell recognition. *Immunol. Today* **11**, 237–244 (1990).
45. Weichold, F. F. *et al.* Regulation of a Graft-Versus-Leukemia Effect by Major Histocompatibility Complex Class II Molecules on Leukemia Cells: HLA-DR1 Expression Renders K562 Cell Tumors Resistant to Adoptively Transferred Lymphocytes in Severe Combined Immunodeficiency Mice/Nonobese Diabetic Mice. *Blood* **90**, 4553–4558 (1997).
46. Xing, S. & Ferrari de Andrade, L. NKG2D and MICA/B shedding: a 'tag game' between NK cells and malignant cells. *Clin. Transl. Immunol.* **9**, e1230 (2020).
47. Konjević, G. M., Vuletić, A. M., Mirjačić Martinović, K. M., Larsen, A. K. & Jurišić, V. B. The role of cytokines in the regulation of NK cells in the tumor environment. *Cytokine* **117**, 30–40 (2019).
48. Holmes, C. & Stanford, W. L. Concise Review: Stem Cell Antigen-1: Expression, Function, and Enigma. *Stem Cells* **25**, 1339–1347 (2007).
49. Bradfute, S. B., Graubert, T. A. & Goodell, M. A. Roles of Sca-1 in hematopoietic stem/progenitor cell function. *Exp. Hematol.* **33**, 836–843 (2005).
50. Hordeaux, J. *et al.* The GPI-Linked Protein LY6A Drives AAV-PHP.B Transport across the Blood-Brain Barrier. *Mol. Ther.* **27**, 912–921 (2019).

51. Park, J. W., Park, J. M., Park, D. M., Kim, D.-Y. & Kim, H. K. Stem Cells Antigen-1 Enriches for a Cancer Stem Cell-Like Subpopulation in Mouse Gastric Cancer. *Stem Cells* **34**, 1177–1187 (2016).
52. Li, Y. *et al.* Evidence that transgenes encoding components of the Wnt signaling pathway preferentially induce mammary cancers from progenitor cells. *Proc. Natl. Acad. Sci. U. S. A.* **100**, 15853–15858 (2003).
53. Roarty, K., Baxley, S. E., Crowley, M. R., Frost, A. R. & Serra, R. Loss of TGF-β or Wnt5a results in an increase in Wnt/β-catenin activity and redirects mammary tumour phenotype. *Breast Cancer Res. BCR* **11**, R19 (2009).
54. Batts, T. D. *et al.* Stem Cell Antigen-1 (Sca-1) Regulates Mammary Tumor Development and Cell Migration. *PLOS ONE* **6**, e27841 (2011).
55. Liu, D. *et al.* A systematic survey of LU domain-containing proteins reveals a novel human gene, LY6A, which encodes the candidate ortholog of mouse Ly-6A/Sca-1 and is aberrantly expressed in pituitary tumors. *Front. Med.* (2023) doi:10.1007/s11684-022-0968-4.
56. Shmerling, M. *et al.* LY6S, a New IFN-Inducible Human Member of the Ly6a Subfamily Expressed by Spleen Cells and Associated with Inflammation and Viral Resistance. *ImmunoHorizons* **6**, 253–272 (2022).
57. Hossiny, M. A. *et al.* Ly6E/K signaling to TGF-β promotes breast cancer progression, immune escape and drug resistance. *Cancer Res.* **76**, 3376–3386 (2016).
58. Shokouhifar, A., Firouzi, J., Nouri, M., Sarab, G. A. & Ebrahimi, M. NK cell upraise in the dark world of cancer stem cells. *Cancer Cell Int.* **21**, 682 (2021).
59. Tsuchiya, H. & Shiota, G. Immune evasion by cancer stem cells. *Regen. Ther.* **17**, 20–33 (2021).
60. Schaloske, R. H. & Dennis, E. A. The phospholipase A2 superfamily and its group numbering system. *Biochim. Biophys. Acta BBA - Mol. Cell Biol. Lipids* **1761**, 1246–1259 (2006).

61. Brown, W. J., Chambers, K. & Doody, A. Phospholipase A2 (PLA2) Enzymes in Membrane Trafficking: Mediators of Membrane Shape and Function. *Traffic* **4**, 214–221 (2003).
62. Jaworski, K. *et al.* AdPLA ablation increases lipolysis and prevents obesity induced by high fat feeding or leptin deficiency. *Nat. Med.* **15**, 159–168 (2009).
63. Jin, K., Qian, C., Lin, J. & Liu, B. Cyclooxygenase-2-Prostaglandin E2 pathway: A key player in tumor-associated immune cells. *Front. Oncol.* **13**, (2023).
64. Take, Y., Koizumi, S. & Nagahisa, A. Prostaglandin E Receptor 4 Antagonist in Cancer Immunotherapy: Mechanisms of Action. *Front. Immunol.* **11**, (2020).
65. Ching, M. M., Reader, J. & Fulton, A. M. Eicosanoids in Cancer: Prostaglandin E2 Receptor 4 in Cancer Therapeutics and Immunotherapy. *Front. Pharmacol.* **11**, (2020).
66. Cózar, B. *et al.* Tumor-Infiltrating Natural Killer Cells. *Cancer Discov.* **11**, 34–44 (2021).
67. Böttcher, J. P. *et al.* NK Cells Stimulate Recruitment of cDC1 into the Tumor Microenvironment Promoting Cancer Immune Control. *Cell* **172**, 1022-1037.e14 (2018).
68. Holt, D., Ma, X., Kundu, N. & Fulton, A. Prostaglandin E2 (PGE2) suppresses Natural Killer cell function primarily through the PGE2 receptor EP4. *Cancer Immunol. Immunother. CII* **60**, 1577–1586 (2011).
69. Pan, D. *et al.* A major chromatin regulator determines resistance of tumor cells to T cell–mediated killing. *Science* **359**, 770–775 (2018).
70. Manguso, R. T. *et al.* In vivo CRISPR screening identifies Ptpn2 as a cancer immunotherapy target. *Nature* **547**, 413–418 (2017).
71. Cucolo, L. *et al.* The interferon-stimulated gene RIPK1 regulates cancer cell intrinsic and extrinsic resistance to immune checkpoint blockade. *Immunity* **55**, 671-685.e10 (2022).
72. Song, M. *et al.* Low-Dose IFNγ Induces Tumor Cell Stemness in Tumor Microenvironment of Non-Small Cell Lung Cancer. *Cancer Res.* **79**, 3737–3748 (2019).
73. Hao, Q. & Tang, H. Interferon-γ and Smac mimetics synergize to induce apoptosis of lung cancer cells in a TNFα-independent manner. *Cancer Cell Int.* **18**, 84 (2018).

74. Su, Q., Wang, F., Dong, Z., Chen, M. & Cao, R. IFN-γ induces apoptosis in human melanocytes by activating the JAK1/STAT1 signaling pathway. *Mol. Med. Rep.* **22**, 3111–3116 (2020).
75. Sironi, J. J. & Ouchi, T. STAT1-induced Apoptosis Is Mediated by Caspases 2, 3, and 7 *. *J. Biol. Chem.* **279**, 4066–4074 (2004).
76. Shen, J. *et al.* Anti-cancer therapy with TNFα and IFNγ: A comprehensive review. *Cell Prolif.* **51**, e12441 (2018).
77. Zaidi, M. R. The Interferon-Gamma Paradox in Cancer. *J. Interferon Cytokine Res.* **39**, 30–38 (2019).
78. ClustVis: a web tool for visualizing clustering of multivariate data using Principal Component Analysis and heatmap | Nucleic Acids Research | Oxford Academic. https://academic.oup.com/nar/article/43/W1/W566/2467929.
79. Federico, A. & Monti, S. hypeR: an R package for geneset enrichment workflows. *Bioinformatics* **36**, 1307–1308 (2019).
80. Berest, I. *et al.* Quantification of Differential Transcription Factor Activity and Multiomics-Based Classification into Activators and Repressors: diffTF. *Cell Rep.* **29**, 3147-3159.e12 (2019).
81. Kulakovskiy, I. V. *et al.* HOCOMOCO: expansion and enhancement of the collection of transcription factor binding sites models. *Nucleic Acids Res.* **44**, D116–D125 (2016).
82. Colaprico, A. *et al.* TCGAbiolinks: an R/Bioconductor package for integrative analysis of TCGA data. *Nucleic Acids Res.* **44**, e71 (2016).
83. Zijlstra, M. *et al.* Beta 2-microglobulin deficient mice lack CD4-8+ cytolytic T cells. *Nature* **344**, 742–746 (1990).
84. Dull, T. *et al.* A Third-Generation Lentivirus Vector with a Conditional Packaging System. *J. Virol.* **72**, 8463–8471 (1998).
85. Pagès, H., Aboyoun, R., Gentleman, R., & DebRoy, S. Biostrings: Efficient manipulation of biological strings version 2.58.0 from Bioconductor. https://rdrr.io/bioc/Biostrings/ (2020).

86. Love, M. I., Huber, W. & Anders, S. Moderated estimation of fold change and dispersion for RNA-seq data with DESeq2. *Genome Biol.* **15**, 550 (2014).
87. Mölder, F. *et al.* Sustainable data analysis with Snakemake. *F1000Research* **10**, 33 (2021).
88. Dobin, A. *et al.* STAR: ultrafast universal RNA-seq aligner. *Bioinformatics* **29**, 15–21 (2013).
89. Patro, R., Duggal, G., Love, M. I., Irizarry, R. A. & Kingsford, C. Salmon: fast and bias-aware quantification of transcript expression using dual-phase inference. *Nat. Methods* **14**, 417–419 (2017).
90. Zhu, A., Ibrahim, J. G. & Love, M. I. Heavy-tailed prior distributions for sequence count data: removing the noise and preserving large differences. *Bioinformatics* **35**, 2084–2092 (2019).
91. Ritchie, M. E. *et al.* limma powers differential expression analyses for RNA-sequencing and microarray studies. *Nucleic Acids Res.* **43**, e47 (2015).
92. Liberzon, A. *et al.* The Molecular Signatures Database (MSigDB) hallmark gene set collection. *Cell Syst.* **1**, 417–425 (2015).
93. Buenrostro, J. D., Wu, B., Chang, H. Y. & Greenleaf, W. J. ATAC-seq: A Method for Assaying Chromatin Accessibility Genome-Wide. *Curr. Protoc. Mol. Biol.* **109**, (2015).
94. Ewels, P. A. *et al.* The nf-core framework for community-curated bioinformatics pipelines. *Nat. Biotechnol.* **38**, 276–278 (2020).
95. Gaspar, J. M. Improved peak-calling with MACS2. 496521 Preprint at https://doi.org/10.1101/496521 (2018).
96. Heinz, S. *et al.* Simple combinations of lineage-determining transcription factors prime cis-regulatory elements required for macrophage and B cell identities. *Mol. Cell* **38**, 576–589 (2010).
97. Quinlan, A. R. & Hall, I. M. BEDTools: a flexible suite of utilities for comparing genomic features. *Bioinforma. Oxf. Engl.* **26**, 841–842 (2010).

98. Liao, Y., Smyth, G. K. & Shi, W. featureCounts: an efficient general purpose program for assigning sequence reads to genomic features. *Bioinformatics* **30**, 923–930 (2014).

99. Thorvaldsdóttir, H., Robinson, J. T. & Mesirov, J. P. Integrative Genomics Viewer (IGV): high-performance genomics data visualization and exploration. *Brief. Bioinform.* **14**, 178–192 (2013).

100. Ewels, P., Magnusson, M., Lundin, S. & Käller, M. MultiQC: summarize analysis results for multiple tools and samples in a single report. *Bioinformatics* **32**, 3047–3048 (2016).

101. Wiśniewski, J. R., Zougman, A., Nagaraj, N. & Mann, M. Universal sample preparation method for proteome analysis. *Nat. Methods* **6**, 359–362 (2009).

102. Block, J. *et al.* Systemic Inflammation and Normocytic Anemia in DOCK11 Deficiency. *N. Engl. J. Med.* (2023) doi:10.1056/NEJMoa2210054.

Figure Legends

Figure 1: Co-culture system to study cancer immunoediting *in vitro*. (A) Scheme illustrates the experimental setup: BCR/ABL^{p185+} B-ALL leukaemic cells (LCs) are transduced with a DNA barcode library. Barcoded LCs are co-cultured with NK cells for 4-20 days *in vitro*. **(B)** Ten B-ALL cell lines were generated from C57BL/6 WT mice and characterised regarding the surface expression of NK ligands (black) and their susceptibility towards NK cell killing (red, depicted here is the cytotoxicity at E:T=10:1) measured by flow cytometry. Cell lines #13 and #15, in blue, showed the highest NK cell susceptibility and were used for the following experiments. Rows were centered; unit variance scaling was applied to rows. Both rows and columns were clustered using correlation distance and average linkage. The plot was generated using the Clustvis web tool[78]. **(C)** B-ALL cell lines were DNA barcoded by lentiviral transduction. Using different amounts of viral supernatant, the optimum transduction efficiency (<5%)[15] was chosen to allow a single barcode integration per cell as determined by GFP expression and measured by flow cytometry. Shown are means±SD (n=2) of one representative cell line. **(D)** Cell lines A-D were analysed for their barcode diversity. Two B-ALL cell lines (#13 and #15) were barcoded (n=2 independent transductions, <5% transduction efficiency) and the barcode diversity of the FACS-purified GFP^{+} cell lines was determined by targeted DNA sequencing. Cell lines A and B are derived from #13 and cell lines C and D from #15. Bars show barcode diversity of barcoded tumour cell lines (A&D n=3 and B&C n=2 independent experiments, each determined by sequencing of 3 biological and 2 technical replicates). Shown is median with interquartile range. **(E)** Barcoded WT B-ALL cell lines A-D (n=4) were cultivated in three individual wells either in the absence or presence of purified and IL-2-activated NK cells. One *B2m*$^{-/-}$ B-ALL cell line was included as control. Absolute numbers of B-ALL cells were determined by flow cytometry. On day 0, 4 and 14, B-ALL cells were FACS sorted, re-plated and fresh NK cells were replenished. Shown are means±SD of n=4 B-ALL cell lines of one representative experiment (n=3 independent experiments); the significance was calculated by an unpaired t-test. **(F)** On day 25, a standard 4h NK cytotoxicity assay was performed using B-ALL cells that had been cultured

for 20 days in the presence or absence of NK cells. Shown are means±SEM of n=4 cell lines (in technical triplicates) of one representative experiment (n=3 experiments); the significance was calculated by a paired t-test.

Figure 2: Quantification of NK cell-mediated cancer immunoediting *in vitro*. (A-B) Schematic representation of the proposed model. Upon long-term co-culture of B-ALL and NK cells, we hypothesised that each tumour cell clone would fall in one of the following categories: The abundance of the clone can be significantly higher (primary resistant) or lower (eliminated), unchanged (static) or show a high variability (secondary resistant). **(B)** A rule-based decision tree was designed to discriminate the four categories depicted in (A). Variability is defined as $v = log2(max(x+1)/min(x+1))$. **(C)** The heatmap shows the normalised abundance of barcodes (norm. BC abundance) of one cell line A (n=3 wells) from one representative experiment (in total: n=4 cell lines, n=2 experiments, n=3 wells, sequenced in technical duplicates). Each column in the figure represents a sample (well), and each row represents a barcode. The barcodes were divided into the four pre-defined groups according to the criteria defined in (B). The Shannon index (shown above the heatmap) serves as measure of barcode diversity and drops significantly after 14 days of NK co-culture. The histogram on the left shows the average abundance of the barcoded cell clone in the B-ALL only samples on day 4. **(D)** The bubble plot depicts the normalised abundance of barcodes of resistant (2nd) clones in B-ALL samples (day 4) compared to B-ALL + NK samples (day 14). The size and colour of the bubbles indicate the normalised barcode abundance. Shown here is the same cell line and experiment as in (C). **(E)** Comparing two individual experiments using the same representative cell line A as shown in (C&D), the Euler diagrams highlight a high overlap of eliminated, resistant (1st), and static cell clones. In contrast, only two resistant (2nd) clones were shared between both independent experiments.

Figure 3: Integrative analysis of RNA-seq and ATAC-seq shows well-known and novel genes deregulated in NK resistant B-ALL cells. The transcriptome **(A-D and G)** and chromatin accessibility **(E-I)** analysis of B-ALL cells co-cultured with NK cells for 4 (time point

1 (TP1)) or 14 (TP2) days were analysed and compared to the non-co-cultured B-ALL cells on TP1 (n=3-4 independent experiments). **(A)** The volcano plot shows the significantly up- or downregulated genes in B-ALL cell lines A and B after co-culture with NK cells for 14 days (n=3 experiments). Statistics were calculated with the Wald test (adjusted p-value (padj)_cutoff < 0.05; $\log_2$FC_cutoff > 0.58 (FC = 2)). **(B)** The dot plot illustrates the enrichment analysis using the hyperR tool[79] for the Gene Ontology Biological Process (GOBP) terms associated with NK co-cultured B-ALL cells shown in panel (A). X-axis and dot colour depicts the false discovery rate (FDR) and y-axis the corresponding biological processes. Dot size illustrates the number of genes associated to the biological processes. **(C)** The Venn diagrams display up- or downregulated genes in cell lines A/B and/or C/D after 14 days of NK co-culture. **(D)** Heatmap shows the expression of selected overlapping genes (top-20 up-regulated, top-10 down-regulated; ranked by p-value) identified in (C) (n=3-4 experiments, 4 B-ALL cell lines). The row-scaled normalized counts represents the $\log_2$(fold change). **(E)** The volcano plot shows differentially accessible chromatin regions in B-ALL cells A and B after co-culture with NK cells for 14 days (n=3 experiments). Statistics were calculated with the Wald test (padj_cutoff < 0.05; $\log_2$FC_cutoff > 0.58 (FC = 2)). **(F)** The Venn diagrams highlights genes whose promoters (TSS +/- 3kb) had higher or lower chromatin accessibility in cell lines A/B and/or C/D after 14 days of NK co-culture in n=3-4 experiments. Gene promoters with the highest |$\log_2$(fold change)| are highlighted. **(G)** Integration of RNA- and ATAC-seq data shows that 37 genes are up- and 16 downregulated in cell lines A/B; the top 10 up- or downregulated genes are highlighted on the right. **(H)** Differential transcription factors (diffTF) analysis[80] highlighted activator (green) and repressor (red) transcription factors (TFs) that are differentially expressed in B-ALL cell lines A and B after NK co-culture (right side of the plot) or B-ALL alone (left side of the plot). **(I)** Integrative Genomics Viewer (IGV) genome browser tracks display representative ATAC-seq signal densities at the *Ly6a* and *Plaat3* loci in B-ALL cells with or without NK co-culture. Shown are the gene bodies including a 3 kb upstream promoter region, as well as binding sites of TFs

identified in (H). Database HOCOMOCO (v10)[81] was used and depicted are counts per million (CPM) with a range of [0-1.37].

Figure 4: NK cell-derived IFN-γ is a major driver of leukaemia immunoediting. (A) Barcoded WT B-ALL cell lines (n=2 cell lines A&D) were cultivated in three individual wells either in the absence or presence of purified and IL-2-activated WT or *Prf1*$^{-/-}$ NK cells or with 2 ng/ml IFN-γ. Absolute numbers of B-ALL cells were determined by flow cytometry. On day 0, 4 and 14, B-ALL cells were FACS sorted, re-plated and fresh NK cells were replenished. Shown are means±SD of n=2 B-ALL cell lines of one representative experiment (n=2 independent experiments). The significance was calculated with the Kruskal-Wallis test and Dunn´s multiple comparisons testing. **(B)** On day 28, a standard 4h NK cytotoxicity assay with WT NK cells was performed using B-ALL cells that had been cultured for 27 days in the presence or absence of NK cells or IFN-γ. Shown are means±SEM of 2 cell lines (in technical triplicates) of one representative experiment (n=2 experiments). Statistics were calculated with a matched two-way ANOVA with Dunnett´s multiple comparisons test. **(C)** B-ALL cells were FACS sorted on day 14, and the barcode diversity was determined by targeted DNA amplicon sequencing. The Shannon diversity of leukaemic clones dropped significantly ($p = 0.0134$) upon co-culture with WT NK cells, and to a lesser degree with *Prf1*$^{-/-}$ NK cells or recombinant IFN-γ. Shown is the mean and dots depict each replicate. Statistics were calculated with the Kruskal-Wallis and Dunn´s multiple comparisons testing. **(D)** The barcodes within each sample were classified according to the decision tree in Fig. 2B. The barcodes that were attributed to the four pre-defined groups were compared between the treatment groups. Heatmaps indicate the number of barcodes shared between treatment groups (bright yellow = high, dark green = low). Resistant (1st) and eliminated leukaemic clones were broadly overlapping between WT or *Prf1*$^{-/-}$ NK- or IFN-γ-treated B-ALL cells. However, resistant (2nd) leukaemic clones were highly specific for each of these conditions. **(E)** The bubble plots show the normalised abundance of barcodes of resistant (2nd) clones in B-ALL samples compared to B-ALL + WT or *Prf1*$^{-/-}$ NK or IFN-γ samples (day 14). The size and colour of the bubbles indicate the barcode abundance. **(F)** The Venn diagram displays

the number up-regulated genes in cell lines A/D after 14 days of co-culture with WT or *Prf1*$^{-/-}$ NK cells or stimulation with recombinant IFN-γ. The orange list highlights the top 10 upregulated genes in the intersection of the three comparisons and the red list shows the WT NK cell specific top 10 upregulated genes. **(G)** The Venn diagram displays the number of downregulated genes in cell lines A/D after 14 days of co-culture with WT or *Prf1*$^{-/-}$ NK cells or stimulation with recombinant IFN-γ. The blue list highlights the top 10 downregulated genes in the intersection of the three comparisons and the red list shows the WT NK cell specific top 10 downregulated genes. (A-G) Shown is one representative experiment (A&B, n=2 cell lines) or one representative cell line from one experiment (C-G, n=2 cell lines).

Figure 5: The role of Ly6A and *PLAAT3* in the evasion of leukaemic cells from NK cell-mediated surveillance. (A and D) Bar graphs show protein abundances of Ly6A and PLAAT3 on day 14 of the same conditions as in the co-culture experiment described in Figure 4. Two B-ALL cell lines (A in circles/D in triangles) were analysed by mass spectrometry in triplicates. Bars represent means; the significance was calculated by one-way ANOVA with Tukey post-hoc test. **(B and E)** *Ly6a* or *Plaat3* KO clones were generated by ribonucleoprotein transfection into parental B-ALL cell lines. The gene modification was verified by TIDE (Tracking of Indels by Decomposition) PCR and sequencing (not shown) as well as by **(B)** measuring Ly6A surface expression by flow cytometry or **(E)** *Plaat3* mRNA expression was analysed by qPCR. Bars and error bars represent means±SD; the significance was calculated using an unpaired t-test. **(C and F)** A 4h standard NK cytotoxicity assay was performed using WT and (C) *Ly6a* or (F) *Plaat3* KO B-ALL clones. The graph shows the summary data of three independent experiments. Shown are means±SEM of n=2 *Ly6a* WT and KO clones (p-value = 1.15e-8) and n=4 *Plaat3* WT and KO cell clones (not significant). The p-value was calculated utilising a t-test after fitting the specific lysis values of the 3 biological replicates on a linear model (more details in the methods section). **(G-I)** Kaplan-Meier plots depicting survival probability of (G) NCICCR-DLBCL, (H) TARGET-AML and (I) TARGET-ALL-P2 patient cohorts (GDC data portal v38.0) divided into *PLAAT3* high and low expressing groups. The cohorts were separated by the modified Z-score (also

known as Median Absolute Deviation); high expression cohort $Z > 1.5$, low expression cohort $Z \leq 1.5$). Analysis was performed with TCGAbiolinks R package[82] and p-value was calculated with a Log-rank test.

Methods

Mice

C57BL/6JRj wild-type mice and C57BL/6-Prf1^{tm1Sdz}/J (*Prf1*$^{-/-}$) mice[26] were obtained from the Jackson Laboratory (Strain #002407). B6.129-B2m^{tm1Jae} (*B2m*$^{-/-}$)[83] mice were kindly provided by Thomas Kolbe (VetMedUni Vienna). The background of the animals was verified as pure C57BL/6 by the GVG Genetic Monitoring GmbH. The mice were between 8 and 12 weeks of age and maintained under specific pathogen-free conditions according to FELASA guidelines.

Cell culture

To generate BCR/ABL^{p185+} (B-ALL) cell lines, bone marrow was isolated from 8-10-week-old mice and single cell suspensions were prepared through repeated homogenisation using 18G and 24G needles. 48 hours before the infection of bone marrow cells, Phoenix-ECO cells were transiently transfected with a retroviral MSCV-BCR/ABL^{p185} vector (kindly provided by Veronika Sexl) mixed with PureFection transfection reagent (System Biosciences). The bone marrow cells were transduced for 1 hour with the fresh viral supernatant in the presence of 10 µg/ml polybrene (Sigma Aldrich) and 10 ng/ml recombinant murine IL-7 (Peprotech). Transformed B-ALL cell lines were maintained in RPMI medium (Thermo Fisher Scientific) supplemented with 100 U/ml penicillin and 100 µg/ml streptomycin (Thermo Fisher Scientific), 10% fetal bovine serum (FBS) (Capricorn) and 50 µM β-mercaptoethanol (Sigma-Aldrich) (cRPMI).

Primary mouse NK cells were isolated from spleens of 8-12-week-old wild-type or *Prf1*$^{-/-}$ mice using the negative selection EasySep mouse NK cell isolation kit (STEMCELL Technologies) or positive selection CD49b (DX5) MicroBeads kit (Miltenyi Biotec) and cultured in cRPMI supplemented with 5,000 U/ml recombinant human IL-2 (Miltenyi Biotec). Mouse NK (mNK) cell purity was measured by flow cytometry with the fixable viability dye eFluor 780 (Invitrogen) and the following antibodies purchased from Miltenyi Biotec: mCD335 (REA815),

mCD45.2 (REA1223), mNK1.1 (REA1162) and mCD3 (REA641). mNK cells were identified by gating on mCD45.2^{+} mCD3^{-} NK1.1^{+} mCD335^{+} cells.

Phoenix-ECO and Lenti-X packaging cells were cultured in DMEM medium (Thermo Fisher Scientific) with 10% FBS.

DNA barcoding

Generation of the lentiviral barcode library LG2.1

The BC1DS_lib oligo containing a 21nt random barcode sequence (**Table S1**) was PCR amplified (14 cycles: 10sec 98°C, 30 sec 57°C, 20 sec 72°C) with Phusion polymerase (New England Biolabs (NEB)). The resulting PCR amplified product was column purified (MinElute PCR cleanup kit, Qiagen) and subsequently digested with XhoI and AscI, followed by ligation into the 3' UTR of the GFP cDNA sequence within the pRRL lentiviral vector, using the Electroligase kit (NEB). Electrocompetent ElectroMax Stbl4 bacteria (Invitrogen) were then electroporated with 6 ng ligation product and a small fraction of the transformed bacteria was plated on Luria-Bertani (LB) agar plates to determine transformation efficiency, while the remaining bacteria were grown overnight in 400 ml LB medium (VWR Life Science) supplemented with 100 µg/ml ampicillin (Sigma Aldrich). DNA was extracted from the bacterial culture using the Maxiprep kit (Invitrogen).[16,84] This barcode library was kindly provided by Ton Schumacher and amplified further to generate our in house library. ElectroMax Stbl4 bacteria were transformed with 10 ng barcode library to achieve a transformation rate of 100 times the estimated barcode diversity of the library. Bacteria were cultured on LB agar medium (bacteriological agar, tryptone, yeast extract (Oxoid) and sodium chloride (Roth)) petri dishes with 100 µg/ml ampicillin and on the next day resuspended in 50 ml LB medium (tryptone, yeast extract and sodium chloride) with 100 µg/ml ampicillin. Bacteria were expanded in up to 400 ml liquid culture. DNA was extracted with EndoFree Plasmid Maxi Kit (Qiagen). To determine the library's barcode diversity and distribution, barcodes were amplified with a three PCR reaction protocol (see below) in biological and technical duplicates and sequenced on a HiSeq 3000/4000 device (Illumina) with 64 bp single-end reads at the Biomedical Sequencing Facility (BSF) Vienna.

Barcoding of tumour cells

Lenti-X cells (Takara Bio) were transfected with the LG2.1 barcode library and the two packaging plasmids p8.9QV (provided by Ton Schumacher) and VSVG (provided by Veronika Sexl) using the PureFection transfection reagent. Virus supernatant was harvested after 48 hours and 72 hours and concentrated with AMICON columns (Sigma Aldrich). $2x10^5$ B-ALL cells were spinfected with serially diluted viral supernatant for 90 minutes at 900xg. The transduction rate (% GFP^+ cells) was measured by flow cytometry 3 days after transduction. Tumour cells with the desired transduction rate (<5%[15]) were expanded and FACS sorted to enrich GFP^+ cells. Barcoded tumour cells were frozen for further experiments.

Flow cytometry

***In vitro* co-culture system and tumour cell growth analysis**

Barcoded B-ALL cells were co-cultured with mNK cells in a effector-to-target (E:T) ratio of 1:1 in three biological replicates per condition. Depending on NK cell cytotoxicity and tumour cell growth, cells were harvested for FACS sorting and further analyses (described below) on day 4 or 6 and for the second time point on day 14 or 16. On the day of harvesting, a fraction of tumour cells was co-cultured for a second or third time with fresh mNK cells (E:T = 1:1). All conditions were cultured in the presence of 2,500 U/ml rhIL-2. Wherever indicated, tumour cells treated with 2 ng/ml mouse IFN-γ (Abcam) every 2nd to 3rd day, while splitting or expanding the tumour cells.

During the co-culture, tumour cell growth was monitored by flow cytometry on a FACSymphony A5 Cell Analyzer device (Becton Dickinson). The following antibodies (clones) were purchased from Miltenyi Biotec: mCD45.2 (REA1223), mNK1.1 (REA1162), mCD3 (REA641) and mCD19 (REA749). Zombie Red (Biolegend) was used as viability dye. The absolute number of B-ALL cells was determined with AccuCheck Counting Beads (Invitrogen). Tumour cells were identified by gating on live $mCD45.2^+$ $mCD19^+$ GFP^+ cells. NK cells were detected by gating on live $mCD45.2^+$ $NK1.1^+$ $mCD3^-$ cells.

Surface marker analysis of tumour cells

Tumour cells were split to $3x10^5$ cells/ml two days before the experiment and 10^6 cells were used for the staining. The following antibodies (clones) were used for the staining: CD48 (REA1238), CD112 (829038), CD137L (REA962), CD154 (REA785), CD155 (REA519), TRAIL-R (CD261) (REA1233), Qa-1b (6A8.6F10.1A6), Qa-2a (REA523), H-2Db (REA1198), H-2Kb (REA619), Rae1 (REA723) and Ly6a/Sca-1 (REA422) purchased from Miltenyi Biotec. Single living cells were gated according to size and granularity in FSC-A, SSC-A and FSC-H plots and cell surface marker expression was quantified median fluorescence intensity (MFI).

Cytotoxicity assay and effector function assay

Cytotoxicity was measured with a flow cytometry-based assay. $5x10^4$ CellTrace Violet (Invitrogen) stained B-ALL cells were seeded in 96-well round bottom plates and IL-2-activated mNK cells added in different E:T ratios (B-ALL: 10:1, 5:1, 1:1) in technical duplicates or triplicates. After 4 hours of incubation at 37°C, cells were washed with PBS, stained with fixable viability dye eFluor 780 (Invitrogen) and fixed with fixation buffer (Biolegend). Subsequently, samples were measured with a HTS plate reader on an LSR Fortessa device (Becton Dickinson). Percentage of specific NK cell lysis was calculated as follows: (% dead tumour cells after co-incubation with NK cells - % spontaneous lysis) / (100 % - % spontaneous lysis).

Multi-omics approaches

10^6 GFP^+ barcoded tumour cells were FACS sorted, washed twice with PBS and snap frozen. DNA and RNA were extracted using the AllPrep DNA/RNA Mini Kit (Qiagen).

The barcoded cell lines A/B and C/D were derived from the cell lines #13 and #15, respectively. Therefore, the RNA and ATAC data sets of A/B and C/D pairs were first analysed separately and later integrated to achieve robust and reliable results.

DNA barcode sequencing

Library preparation for barcode sequencing was performed in technical duplicates with three nested PCR steps. PCR#1 amplified the barcodes, PCR#2 added the required sequences for the universal Illumina adapters and four random base pairs (bps) (BC1v2DS For) for a more

diverse sequencing start. PCR#3 attached the P5 and P7 universal Illumina adapters and with the P7 a sample-specific index sequence (Primer sequences and PCR setting information are in **Table S1**). The PCR#3 product fragment size (322 bps) was confirmed on a 2% agarose gel electrophoresis for every sample. The samples were cleaned up with Agencourt AMPure XP beads (Beckman Coulter). Up to 96 equimolar pooled samples spiked with 10-15% PhiX (Illumina) were sequenced with the MiSeq Reagent Kit v3 (Illumina) 64 bp single-end reads with an aimed coverage of 50 to 100 reads/barcode.

Barcode/Cell clone evolution analysis

The R statistics software v4.0.3 was used to analyse barcode abundance and clonal diversity. Unmapped reads were loaded from FASTQ format (function *readDNAStringSet* from package Biostrings v2.58.0[85]) into the R environment. First, we located the barcode sequences by pattern matching (function *vmatchPattern* from package Biostrings v2.58.0) to identify the fixed head ("GAACACTCGAGATCAG") and non-variable ("TGTGGTATGATGT") portions of the reads, which directly enclose the barcodes from left and right, respectively. We then extracted the stretch of sequence in between. Sequences that did not meet the expected length (21 bases) or included uncalled bases ("N") were discarded (mean > 85%, **Table S2**). To define the barcodes of the reference library (**Figure S1C-E**), we selected sequences with a sum of at least 100 reads across samples (n = 4) of the viral library for further analysis. With these we constructed a count matrix indicating the number of reads matching to each barcode. Next, the technical replicates were merged by adding up the read counts. For each cell line, only barcodes detected across three B-ALL alone samples at the first time point (TP1) or at the second time point (TP2) with a total sum of at least 9 reads were considered for downstream analysis (**Table S3**). Barcode diversity for each sample was quantified using Shannon diversity as follows $sum(p * log(p), na.rm = TRUE) * -1$, where p is the ratio of the counts of each barcode out of the total barcode counts. We used DESeq2[86] v1.30.0 to find the subset of differentially abundant barcodes (abs[$\log_2$(fold change]_cutoff) ≥ 1 & padj_cutoff < 0.05) across time point and conditions of interest. Shifted $\log_2$ transformation was used for normalisation (function *normTransform* from package

DESeq2 v1.30.). Based on the statistics of differential abundance and variability across samples (here, the variability was calculated as following: $v = log2(max(x+1)/min(x+1))$, where x is a vector of normalised counts across samples) at every time point. Barcodes were assigned to one of five categories: i) primary resistant: differentially abundant (padj < 0.05) and increasing (log_2(fold change) ≥ 1; comparing B-ALL + NK vs B-ALL alone); ii) eliminated: differentially abundant (padj < 0.05) and decreasing (log_2(fold change) ≤ -1; comparing B-ALL + NK vs B-ALL alone); iii) static: variability v ≤ 0.5 in B-ALL alone, and v < 1 at TP 2; iv) secondary resistant: low variability in B-ALL alone v ≤ 0.5, high variability in B-ALL + NK TP2 v ≥ 1 and barcode abundance high in only one of the three replicates at TP2; v) others: none of the above. Barcodes were further ordered using hierarchical clustering (function *hclust* from package *stats* v 4.0.3, method = "ward.d2"). Heatmaps were generated using ComplexHeatmap v2.7.5.1 and bubble plots were generated using ggplot2 v3.3.3.

RNA sequencing

After RNA isolation (see above), samples were treated with DNase I (Thermo Fisher Scientific). Library preparation and sequencing was performed at the Biomedical Sequencing Facility of the CeMM Research Center for Molecular Medicine of the Austrian Academy of Sciences (BSF).

The amount of total RNA was quantified using the Qubit 4.0 Fluorometric Quantitation system (Thermo Fisher Scientific) and the RNA integrity number (RIN) was determined using the 2100 Bioanalyzer instrument (Agilent). RNA-seq libraries were prepared with the QuantSeq 3‘ mRNA-Seq Library Prep Kit (FWD) for Illumina (Lexogen). Library concentrations were quantified with the Qubit 4.0 Fluorometric Quantitation system and the size distribution was assessed using the 2100 Bioanalyzer instrument. For sequencing, samples were diluted and pooled into NGS libraries in equimolar amounts. Expression profiling libraries were sequenced on HiSeq 3000/4000 or Novaseq 6000 instruments (Illumina) following a 50-base-pair and 120-base-pair single-end setup, respectively. Raw data acquisition and base calling was performed on-instrument, while the subsequent raw data processing off the instruments involved two custom programs based on Picard tools

(2.19.2). In a first step, base calls were converted into lane-specific, multiplexed, unaligned BAM files suitable for long-term archival (IlluminaBasecallsToMultiplexSam, 2.19.2-CeMM. In a second step, archive BAM files were demultiplexed into sample-specific, unaligned BAM files (IlluminaSamDemux, 2.19.2-CeMM).

RNA-seq analysis

The obtained raw reads were processed using the Snakemake pipeline[87]. Mapping of the reads was performed using STAR[88] (v2.7.10a) to the Genome Reference Consortium Mouse Build 38 (GRCm38), and duplicate reads were identified with Picard (v2.27.4). Quantification of the mapped reads was carried out using Salmon[89] (v1.8.0). The following data processing and visualisation was performed in R (v4.2.0). To ensure robustness of the analysis, the data set was filtered to include only transcripts detected in at least three samples. The analysis of cell lines A and B (both established from cell line #13) was performed separately from the analysis of cell line C and D (both originating from cell line #15). Finally, the results were compared.

For count normalisation, variance stabilization, and differential expression analysis, the Bioconductor DESeq2[86] (1.38.3) package was used. DESeq2 employs a negative binomial distribution-based model, with additional shrinkage using apeglm[90] algorithm (v1.20.0). Transcripts were considered significantly differentially expressed between groups of comparison if they exhibited a $\log_2$(fold change) ≥ 0.58 and a padj ≤ 0.05. Only these transcripts were selected for subsequent analysis steps.

The initial exploratory analysis included principal component analysis (PCA), production of expression heatmaps and volcano plots using ggplot2 (v3.4.2) and heatmap (v1.0.12). To correct for batch effects between different experiments in PCA plots (**Figures S3A&B, S4A**) the limma R[91] package (v3.54.2) was utilised. The resulting gene lists were annotated and subjected to gene set enrichment analysis (GSEA). Visualisation of the GSEA results was achieved using the hypeR[79] package (v2.0.1) and represented as dot plot. Gene Ontology Biological Process (GOBP) terms were obtained from the Molecular Signatures Database (MSigDB) using the msigdbr[92] (v7.5.1) package.

ATAC sequencing

50,000 GFP$^+$ tumour cells were FACS sorted into 1.5 ml micro centrifuge tubes containing 400 µl PBS (Sigma Aldrich) and 0.5% Bovine Serum Albumin (BSA, GE Healthcare) and pelleted. Cell lysis and DNA tagmentation was performed in a total volume of 25 µl of 2x TD (Tagment DNA Buffer) and TDE1 (Tagment DNA enzyme) (Illumina), 1% Digitonin (Promega) and 50x EDTA-free Protease Inhibitor Cocktail (Roche) for 30 minutes at 37°C. Samples were purified with the Qiagen MinElute kit (Qiagen). Libraries were generated as described by Buenrostro et al[93] by using the Ad1_noMx and Ad2.1-Ad2.48 indexed primers (**Table S1**). PCR products were purified with Agencourt AMPure XP beads and sample profile was analysed with the High Sensitivity D5000 kit (Agilent Technologies) on a TapeStation (Agilent Technologies). 45-48 equimolar pooled samples were sequenced on a NovaSeq 6000 instrument with 50 bp paired-end reads at the BSF.

ATAC-seq analysis

The obtained raw reads were processed using the ATAC-seq Next Flow[94] pipeline (v2.0). This included mapping the reads with STAR to the GRCm38 genome, identification of duplicates with Picard (v2.27.4), calling broad peaks with MACS2[95] (v2.2.7.1). Peaks overlapping with blacklisted (GRCh38) regions were filtered out and the remaining peaks were annotated with HOMER[96] (v 4.11). Consensus peaks across all samples were identified with BEDTools[97] (v2.30.0) and counting reads in these peaks was done with featureCounts[98] (Rsubread v2.0.1). Visualisation of the ATAC-seq peaks was performed by creation of BigWig files with bedGraphToBigWig (v377) and the following export to IGV[99] browser (v2.16.1). Quality of the obtained raw data was assessed with MultiQC[100] (v1.13). The following data processing and visualisation was performed in R (v4.2.0). To ensure robustness of the analysis, the data set was filtered to include only consensus peaks detected in all three replicates of each condition and cell line and only the peaks that were located in the window of ±3kb around transcription start site (TSS). The analysis of cell lines A and B was performed separately from the analysis of cell line C and D.

Similar to the RNA-seq analysis, the Bioconductor DESeq2 (1.38.3) package was used for counts normalisation, variance stabilisation, and analysis of differential accessibility. Peaks were considered significantly accessible between groups of comparison if they exhibited a $\log_2$(fold change) ≥ 0.58 and a padj ≤ 0.05. Exploratory analysis included PCA, production of heatmaps, volcano plots and GSEA.

Integration of RNA-seq and ATAC-seq data

To integrate two datasets and perform genome-wide quantification of differential transcription factor activity in cell lines at different time points we used diffTF[80] (v1.8). The processing was done only for A and B data sets, due to very high computational demand of the algorithm. The input consisted of raw ATAC-seq reads in BAM files, filtered consensus peaks from the previous step, raw RNA-seq counts, and PWM data for all TFs – HOCOMOCO[81] (v10).

2D-RP/RP Liquid Chromatography – Tandem Mass Spectrometry analysis

Cells were lysed in 200 µL lysis buffer (50 mM HEPES pH 8.0, 2% SDS, 1 mM PMSF, cOmplete Protease Inhibitor Cocktail, Roche), heated to 99 °C for 5 min, and DNA was sheared using a Covaris S2 ultrasonicator. Lysates were cleared at 20,000 × g for 15 min at 20 °C and tryptic digest was performed using FASP according to Wisniewski et al[101]. Peptides were desalted (C18 SPE; Pierce peptide desalting columns, Thermo Fisher Scientific), labeled with TMTpro™ 16plex reagents according to manufacturer´s instructions (Thermo Fisher Scientific), pooled, dried in a vacuum concentrator, and cleaned up via C18 SPE. After re-buffering in 10 mM ammonium formiate buffer pH 10 peptides were fractionated via a C18 column (150 × 2.0 mm Gemini-NX, 3 µm, C18 110Å, Phenomenex, Torrance, CA, USA) on a Dionex UltiMate 3000 nanoLC (Thermo Fisher Scientific). Fractions were dried in a vacuum concentrator and taken up in 0.1% TFA before analysis.

Mass spectrometry analysis was performed on an Orbitrap Fusion Lumos Tribrid mass spectrometer (Thermo Fisher Scientific) coupled to a Dionex UltiMate 3000 nanoLC system (Thermo Fisher Scientific) via a Nanospray Flex Ion Source (Thermo Fisher Scientific) interface using the same procedure as Block et al[102]. Data analysis was performed using the Proteome Discoverer v.2.4.1.15 platform.

Genome editing

Ribonucleoprotein (RNP)-mediated CRISPR genome editing of B-ALL cells

RNP electroporation: crRNAs, Alt-R CRISPR Cas9 tracrRNA ATTO 550 and Alt-R S.p. Cas9-GFP V3 were purchased by Integrated DNA Technologies (IDT). Cells were transfected according to manufacturer´s instructions using the following electroporation settings: 350 V, 5 ms and 1 pulse with the Gene Pulser Xcell electroporation system (BioRad). crRNA sequences: *Ly6a*: TCACGTTGACCTTAGTACCC; TATTGAAAGTATGGAGATCC, *Plaat3*: CGTCATGTTTGTTATTGACC; ATGGCCCAGTGTCTGTACAT. The next day tumour cells were FACS sorted for GFP and ATTO 550 double positivity. After assessing editing efficiency by TIDE sequencing (described below) of the bulk population, cells were single cell FACS sorted into 96-well flat bottom plates into 50% 48 hours old medium of tumour cells and 50% fresh cRPMI. After the outgrowth of single clones, the KO was validated by TIDE sequencing. Therefore, up to 200,000 cells were pelleted and lysed in 50 µl Pawel´s buffer (50 mM potassium chloride (Roth), 10 mM Tris-HCl pH9 (Sigma Aldrich), 0.45% Nonidet-p40 (Calbiochem), 0.45% Tween 20 (Sigma), 0.8 mg/ml proteinase K (Biozym) in deionized water) at 56°C for 15 minutes with subsequent heat inactivation at 95°C for 5 minutes. After centrifugation at 2000xg for 5 minutes, supernatant was used for the TIDE PCR to amplify the breakpoints of the guide RNAs (primer sequences in **Table S1**). PCR products were Sanger sequenced (Microsynth) and analysed for their genotype with the TIDE (nki.nl) web tool. Gene knockouts were validated using flow cytometry (described above) or quantitative PCR (described below).

Quantitative PCR

For the validation of the *Plaat3* expression of tumour cells, RNA of $2x10^6$ cells was extracted with the Monarch Total RNA Miniprep Kit with “on column” DNase I treatment (NEB), cDNA was generated by using LunaScript RT SuperMix Kit (NEB) and qPCR was performed with the Luna universal qPCR Master Mix (NEB) (primer sequences in **Table S1**).

IFN-γ ELISA

Tumour cells were split to $3x10^5$ cells/ml on day 0 and cultivated for 48 hours in cRPMI. On day 2, the supernatant was harvested, filtered through a 45 µm filter, and transferred onto IL-2 expanded mNK cells in the presence of 2,500 U/ml IL-2. After 48 hours, mNK cells were harvested and the supernatant was frozen at -80°C. As positive control served the stimulation of mNK cells with PMA/Ionomycin (Invitrogen) 4 hours before the supernatant harvesting. The ELISA was performed according to manufactures protocol (Abcam) and analysed using the analysis tool: “https://www.arigobio.com/elisa-analysis”.

Statistical analysis

Statistical analysis was performed using GraphPad Prism version 8.4.3 for Windows (GraphPad Software; http://www.graphpad.com) using two-tailed unpaired t-tests, one-way, two-way ANOVA or Kruskal-Wallis test. Where ANOVA showed a statistical difference, Tukey’s multiple comparison testing or Dunnett’s post-hoc testing was applied. The α level for all tests was set to 0.05, and p values were two tailed. The significance level is indicated for each experiment (in general: *$p < 0.05$; **$p < 0.01$; ***$p < 0.001$; ****$p < 0.0001$).

To pool the data from independent cytotoxicity assays (n=3 experiments, Figure 5B), a linear model with the categorical variables ‘Experiment’, ‘E:T Ratio’, ‘Genotype’, ‘Cell line’ and ‘Replicate’ as predictors for the cytotoxicity response was fit using the R function ‘lm’ which performs a t-test to determine significance of the relationship between the predictor variables and the response variable. For visualisation purposes, the effect of experimental batch on the cytotoxicity response was corrected for by subtracting the estimated linear model coefficients for experiments 2 and 3 from the observed specific lysis values of the respective experiments, as the approach used in the ‘removeBatchEffect’ function from the R package limma.

To generate the heatmap in Figure 1B, the data was pooled from two independent experiments by calculating the mean surface marker expression or mean % specific lysis at E:T=10:1. The values were standardised for each variable (row) using the following

calculation: Z-score = (mean of observed values – mean of the samples) / (standard deviation of the samples).

Heatmaps in Figure S6D&H were generated by using the R package ComplexHeatmap (version 2.10.0). The raw median fluorescence intensity (MFI) values minus the MFI of their unstained control served as input. Rows (surface markers) were scaled and clustered (unsupervised). Columns (cell lines) were ordered by genotype and cell line.

Data and code availability

The data and codes generated in the current study are available at Github (https://github.com/TumorImmunoEditingLab). All other relevant data are available from the corresponding author.

Antibody table

Table S4

Acknowledgements

We thank Veronika Sexl from the University of Veterinary Medicine Vienna (VetMedUni Vienna, Austria) for providing the BCR/ABL construct and Thomas Kolbe (VetMedUni Vienna, Austria) for providing the *B2m*$^{-/-}$ mice. We are grateful to Marcus Tötzl and Anastasiya Hladik for their assistance with ATAC-seq library preparation and mouse experiments, respectively. We thank the CCRI FACS and Bioinformatics Core Units for assistance with cell sorting and bioinformatics/statistics, respectively, the Core Facility Laboratory Animal Breeding and Husbandry of the Medical University of Vienna (MUW, Austria) for taking care of our mice and the Biomedical Sequencing Facility and the Proteomics Facility of the CeMM Research Centre for Molecular Medicine of the Austrian Academy of Sciences for their support on next-generation sequencing and mass spectrometry analysis, respectively. This work was supported by the St. Anna Children's Cancer Research Institute (Vienna, Austria), a DOC fellowship of the Austrian Academy of Sciences awarded to M.C.B., and grants from the Austrian Science Fund (P32001-B,

P34832 and WKP132-B) and the Fellinger Krebsforschung to E.M.P. F.H. is supported by funding from the Alex's Lemonade Stand Foundation for Childhood Cancer (20-17258), and the Austrian Science Fund (TAI 454, TAI 732).

Author contributions

Conceptualization: E.M.P.

Methodology: M.C.B., B.K., E.M.P., with input from J.U., J.C., L.P., T.S., D.G.,

Formal analysis: M.C.B., M.R.S, A.B., P.R., E.M.P.

Investigation: M.C.B., H.B., A.D., F.O.D., B.K., F.H.-G., L.S., S.S., D.E., D.G.

Writing (original draft): M.C.B., E.M.P.

Visualization: M.C.B., M.R.S., A.B., E.M.P.

Resources: J.U., J.C., M.L., L.P., T.S., F.H., E.M.P.

Supervision: F.H., E.M.P.

Funding acquisition: M.C.B., E.M.P.

All authors reviewed and edited the manuscript.

Competing interest declaration

The authors declare no competing interests.

Additional information

Corresponding author: Eva Maria Putz, St. Anna Children's Cancer Research Institute (CCRI), Zimmermannplatz 10, 1090 Vienna, Austria, E-mail: eva.putz@ccri.at

Supplementary data figure legends

Supplementary Figure 1: *B2m*$^{-/-}$ B-ALL cell line characterisation and details about the barcode library. (A) Ten *B2m*$^{-/-}$ B-ALL cell lines were generated from B6.129-B2m^{tm1Jae} (*B2m*$^{-/-}$) mice and characterised regarding the surface expression of NK cell ligands and their susceptibility towards NK cell killing (depicted here is the cytotoxicity at E:T=10:1). Rows

were centred; unit variance scaling was applied to rows. Both rows and columns were clustered using correlation distance and average linkage. The plot was generated using the Clustvis web tool[78]. **(B)** Plasmid vector map of the pRRL-CMV-*GFP*-BCv2AscI barcode library plasmid. In the inner circle the CMV promoter, the *GFP* gene, barcode nucleotides (n=20) with Toplib and Botlib primers and the ampicillin resistance are highlighted. Restriction enzyme sites are depicted on the outer circle. **(C)** The barcode library was deep sequenced in technical replicates after plasmid transformation, MaxiPrep and following a 3-step nested PCR library preparation protocol. After raw data processing and filtration for valid barcodes, the barcodes of the technical replicates were compared and overlapped well. Common barcodes are shown in orange; non-overlapping barcodes from replicates 1 or 2 are show in blue or green, respectively. **(D)** The graph shows a representative sequence of one replicate of the barcode library (n=4). Positions 1-4 represent the random nucleotide insertion after using the BC1v2DS_For primer in PCR#2. Positions 5-23 and 44-65 are the constant sequences before and after the barcode, respectively. The 20 nucleotides from positions 24-43 represent the barcode sequence with a similar probability of all four bases to be present at a distinct position. **(E)** The barcode reference library generated in-house (Putz laboratory) was compared to the one used in the Périe laboratory. Both libraries, which were sequenced independently, were overlapping to a high degree. The Putz library detected more barcodes, which was likely due to the higher sequencing depth.

Supplementary Figure 2: Extended quantification of NK cell-mediated cancer immunoediting *in vitro*. According to our hypothesis, the abundance of each barcoded tumour cell clone can be significantly higher (primary resistant) or lower (eliminated), unchanged (static) or show a high variability (secondary resistant) after extended NK cell co-culture. **(A)** The percentage of the cell clones in each group on day 14 is depicted for cell lines A (as shown in Figure 2), B, C and D. Each dot represents the summarised analysis of one independent experiment (plated in three biological replicates and sequenced in technical duplicates). **(B)** Each experiment was performed at least two times using the same barcoded parental cell line. The Euler diagrams compare two individual experiments of cell lines B, C

and D (A is shown in Figure 2). The tumour cell clones that were categorised as eliminated, primary resistant, and static showed a relatively high overlap between the two independent experiments. In contrast, secondary resistant clones were less likely to stem from the same original clone when comparing independent experiments.

Supplementary Figure 3: Analysis of differentially expressed and accessible genes in NK cell resistant tumour cells. (A&B) The principal component analysis (PCA) plot illustrates the transcriptomic relatedness among cell lines **(A)** A and B and **(B)** C and D and conditions (B-ALL alone, B-ALL + WT NK cells on time point 1 (TP1) and time point 2 (TP2)) in the long-term co-culture experiments, summarising 3 or 4 independent experiments, respectively. Data was batch corrected for experiments. **(C)** Volcano plot of the RNA-seq analysis of cell lines C and D showing DEGs of B-ALL + WT NK co-cultured cells (TP2) versus B-ALL alone samples. **(D&E)** The heat maps summarise DEGs of cell lines **(D)** A and B (n=3 experiments) and **(E)** C and D (n=4 experiments). Heat maps were clustered by condition, cell line and experiment. Z-score $\log_2$(fold change) is shown and up- or downregulated genes are depicted in red and blue colour, respectively. **(F&G)** PCA plots from the ATAC-seq analysis compares the similarities of the chromatin accessibility of the cell lines and the different conditions. Cell lines A and B are shown in **(F)** and C and D in **(G)** summarising 3 and 4 independent experiments, respectively. **(H)** The DARs in B-ALL + WT NK cells at TP2 versus B-ALL alone at TP1 were compared and are shown in a volcano plot summarising 4 independent experiments using cell lines C and D.

Supplementary Figure 4: Transcriptomic profiles of tumour cells co-cultured with WT NK cells or *Prf1*$^{-/-}$ NK cells or treated with IFN-γ. (A) PCA analysis of the transcriptomic data from RNA-seq shows that the B-ALL cells treated with IFN-γ possess the most unique transcriptome and form a cluster on their own in both cell lines (A and D). Data was batch corrected for experiments. **(B-D)** Volcano plots showing DEGs of the three treatment conditions (B-ALL + WT NK, B-ALL + *Prf1*$^{-/-}$ NK and B-ALL + IFN-γ) compared to the B-ALL alone samples. Analysis includes both cell lines. Differentially up- or downregulated genes are depicted in red and blue, respectively. **(E-G)** Heat maps depicting all up- or

downregulated genes of the above-mentioned comparisons. Heat maps were batch-corrected for cell line and clustered by cell line and condition. Z-score log_2(fold change) shows the expression of genes from low to high expression depicted with a colour bar from blue to red.

Supplementary Figure 5: NK cell-derived IFN-γ is a major driver of leukaemia immunoediting. (A) The barcoded *B2m*$^{-/-}$ B-ALL cell line was cultivated in three individual wells either in the absence or presence of purified and IL-2-activated WT or *Prf1*$^{-/-}$ NK cells or with 2 ng/ml IFN-γ. Absolute numbers of B-ALL cells were determined by flow cytometry. On day 0, 4 and 14 B-ALL cells were FACS sorted, re-plated and fresh NK cells were replenished. Shown is one representative experiment (n=2 independent experiments). **(B)** On day 28, a standard 4h NK cytotoxicity assay was performed using *B2m*$^{-/-}$ B-ALL cells that had been cultured for 27 days in the presence or absence of NK cells or IFN-γ. Shown are means±SD of one cell line in technical triplicates of one representative experiment (n=2 experiments).

Supplementary Figure 6: Characterisation of *Ly6a* and *Plaat3* KO clones. (A) Growth curve of *Ly6a* WT and KO clones (n=2 per genotype) in absolute cell numbers over 13 days. **(B)** Cell viability of *Ly6a* WT and KO clones (n=2 per genotype) over 13 days measured by Casy cell counter (OLS OMNI Life Science). **(C)** Measurement of IFN-γ secretion by mNK cells upon culturing in tumour cell-conditioned medium for 48 h. As positive control mNK cells were activated with PMA/Ionomycin (n=2 clones per genotype and all conditions were in technical duplicates). **(D)** *Ly6a* WT and KO B-ALL cell lines (n=4 per genotype) were characterised by their surface expression of NK ligands by flow cytometry. Columns represent different tumour cell clones ordered according to genotype and cell line. Data has been both scaled and clustered by row to highlight variations in marker expression across different samples. Red indicates higher and blue lower expression levels of surface ligands. **(E)** Growth curve of *Plaat3* WT and KO clones (n=4 per genotype) showing the proliferation in absolute cell numbers over 13 days. **(F)** Cell viability of *Plaat3* WT and KO clones (n=4 per genotype) measured over 13 days by Casy cell counter. **(G)** Measurement of

IFN-γ secretion by mNK cells upon culturing in tumour cell conditioned medium for 48 h. As positive control mNK cells were activated with PMA/Ionomycin (n=4 clones per genotype and all conditions were in technical duplicates). **(H)** *Plaat3* WT and KO B-ALL cell lines (n=4 per genotype) were characterised regarding the surface expression of NK ligands by flow cytometry and the heat map was generated as described in **(D)**.

Figure 1

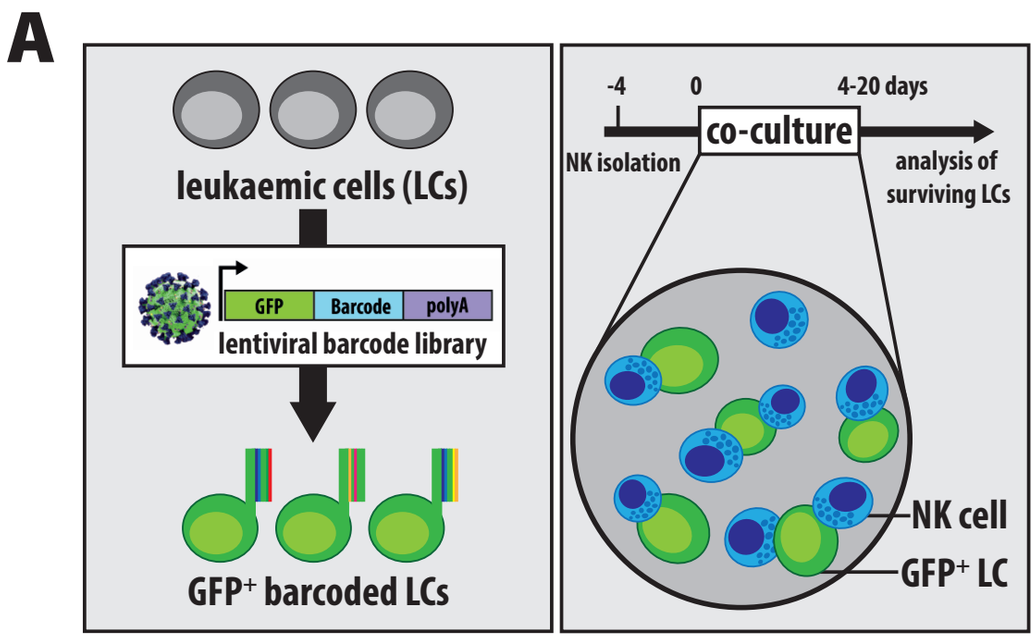
A
leukaemic cells (LCs)
GFP
Barcode
polyA
lentiviral barcode library
GFP+ barcoded LCs
-4
0
4-20 days
co-culture
NK isolation
analysis of surviving LCs
NK cell
GFP+ LC

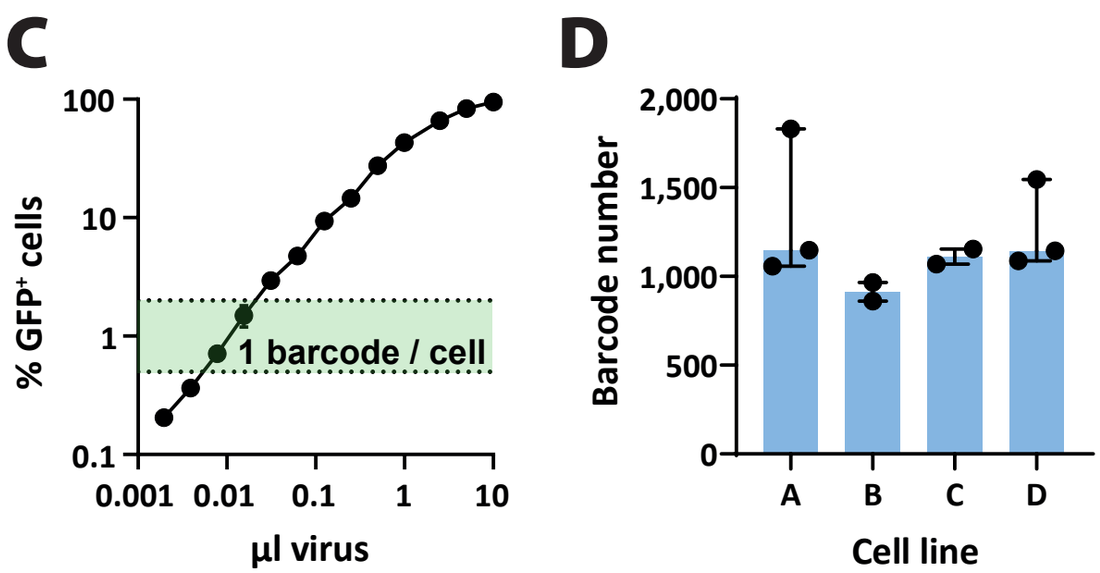
C
% GFP+ cells
100
10
1
0.1
1 barcode / cell
0.001
0.01
0.1
1
10
µl virus
D
Barcode number
2,000
1,500
1,000
500
0
A
B
C
D
Cell line

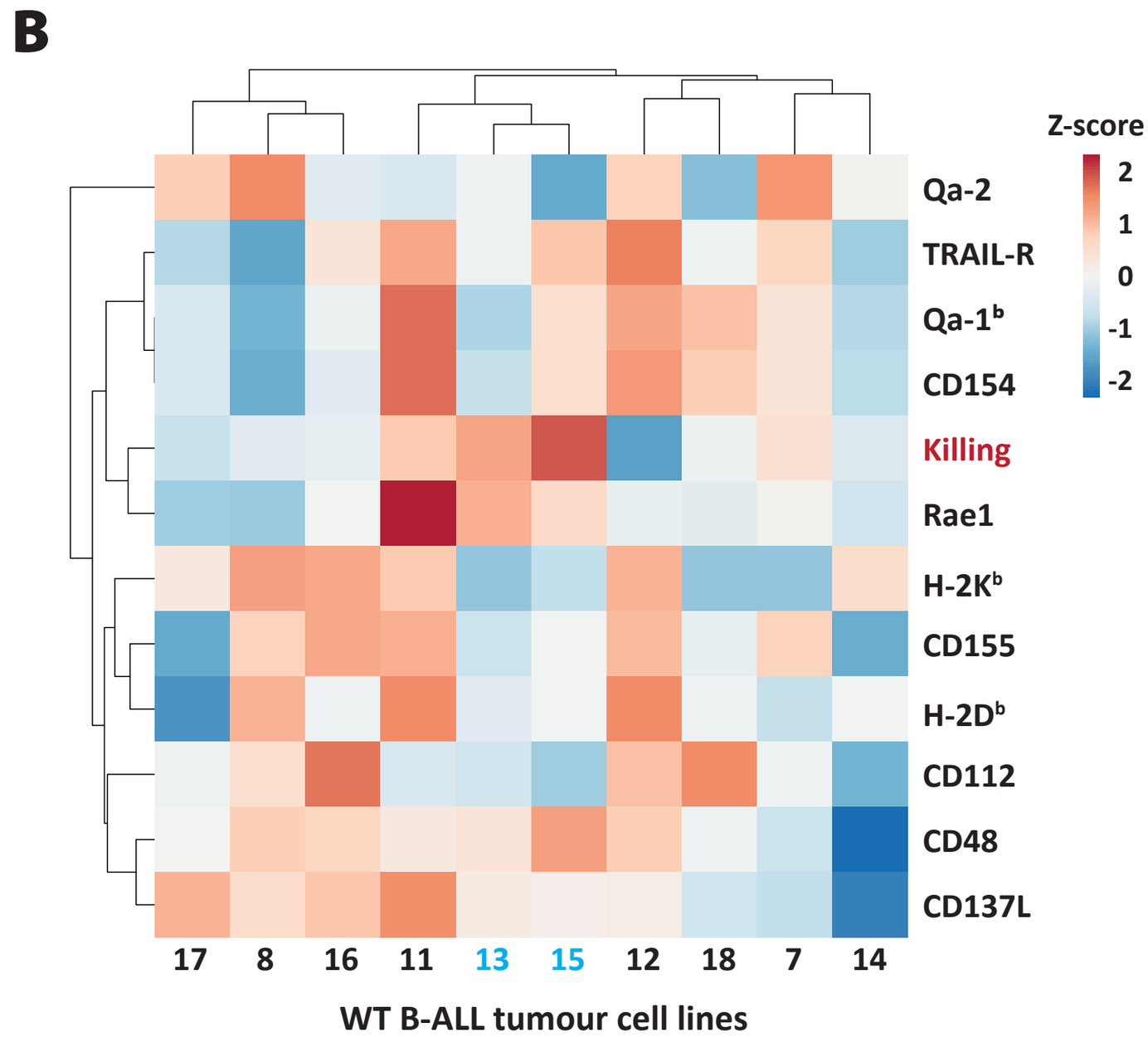
B
Z-score
2
1
0
-1
-2
Qa-2
TRAIL-R
Qa-1b
CD154
Killing
Rae1
H-2Kb
CD155
H-2Db
CD112
CD48
CD137L
17
8
16
11
13
15
12
18
7
14
WT B-ALL tumour cell lines

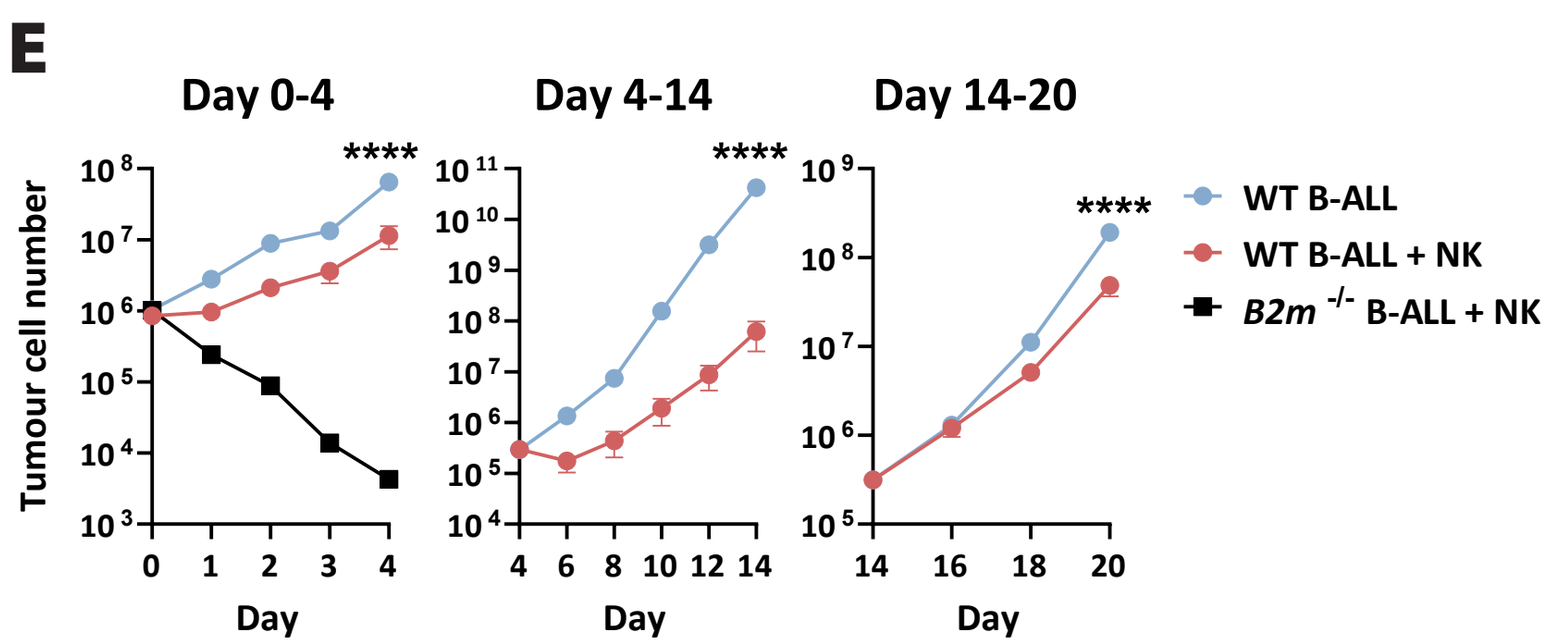
E
Day 0-4
Day 4-14
Day 14-20
Tumour cell number
****
Day
WT B-ALL
WT B-ALL + NK
B2m -/- B-ALL + NK

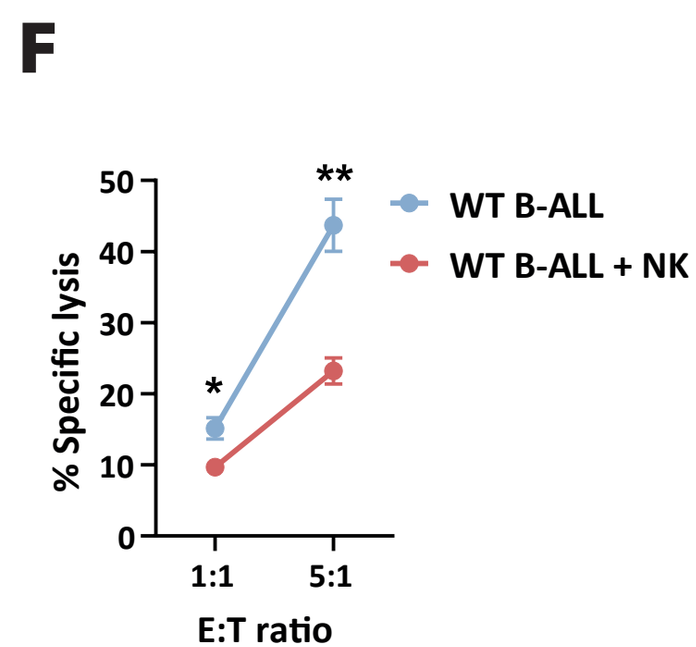
F
% Specific lysis
**
*
1:1
5:1
E:T ratio
WT B-ALL
WT B-ALL + NK

Figure 2

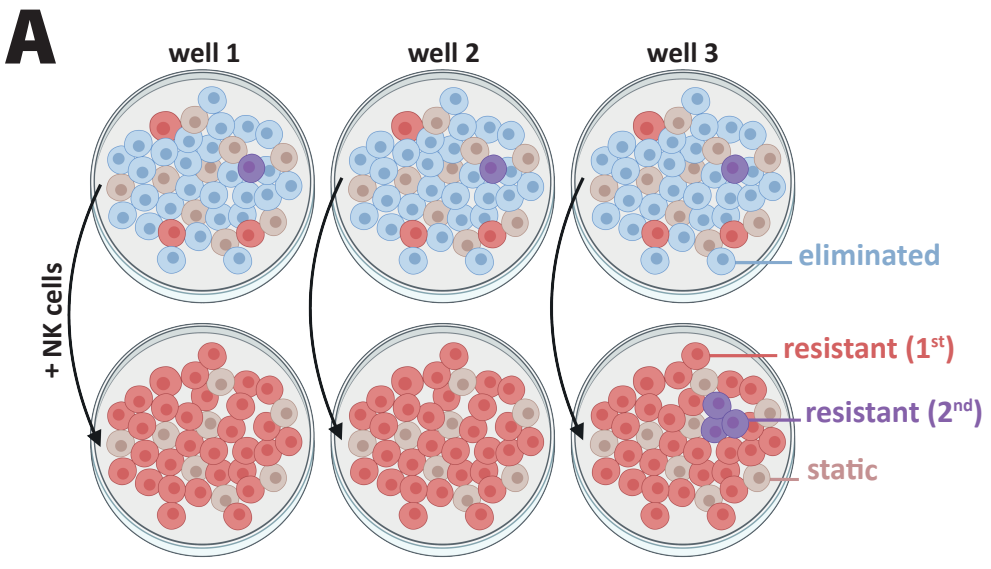
A
well 1
well 2
well 3
+ NK cells
eliminated
resistant (1st)
resistant (2nd)
static

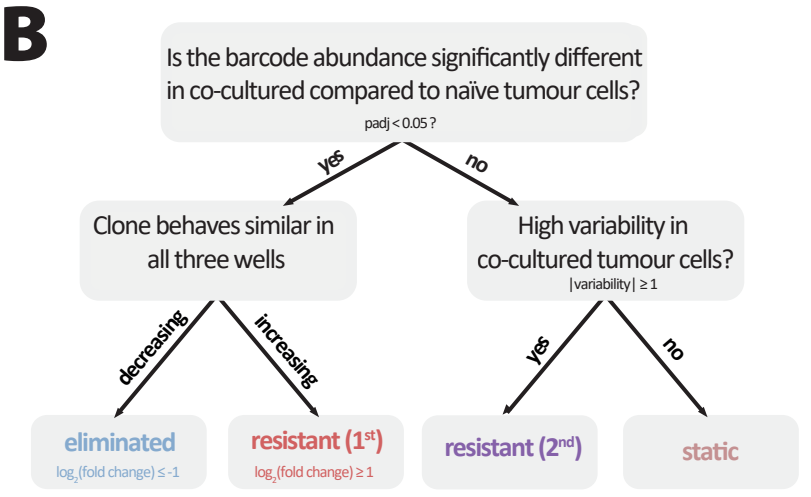
B
Is the barcode abundance significantly different in co-cultured compared to naïve tumour cells?
padj < 0.05 ?
yes
no
Clone behaves similar in all three wells
High variability in co-cultured tumour cells?
|variability| ≥ 1
decreasing
increasing
yes
no
eliminated
log2(fold change) ≤ -1
resistant (1st)
log2(fold change) ≥ 1
resistant (2nd)
static

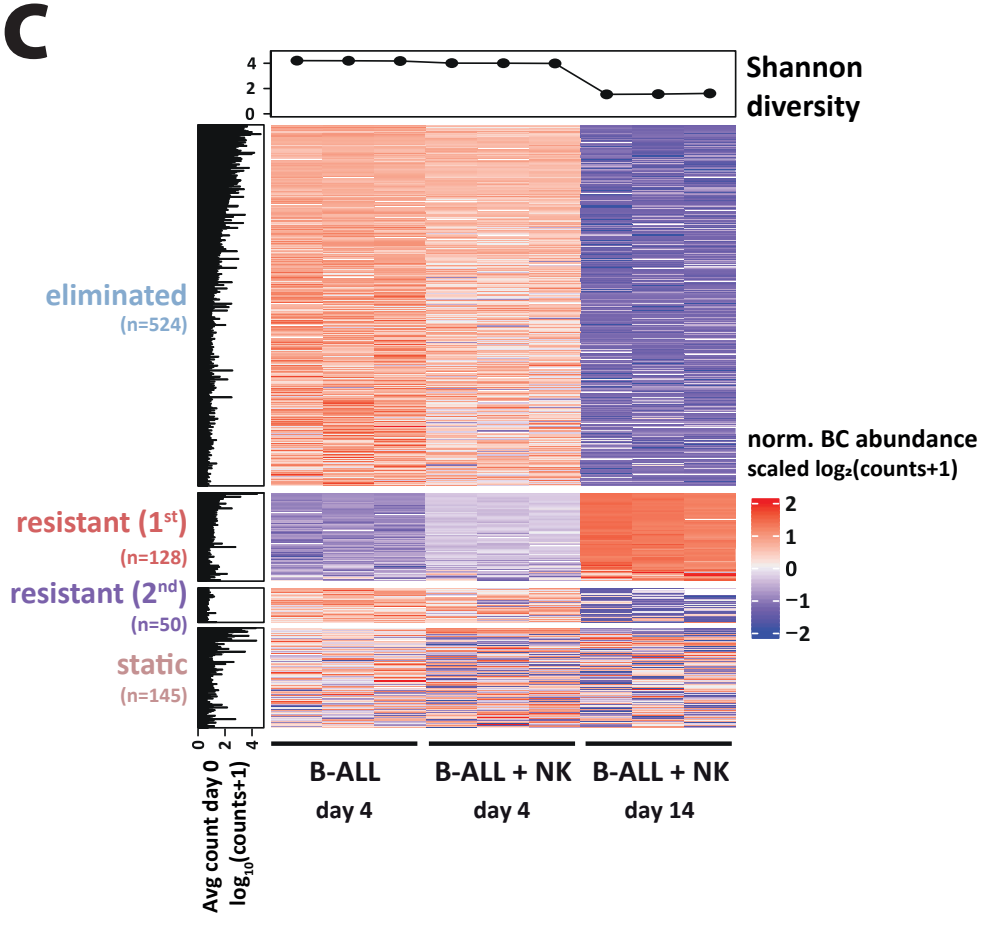
C
Shannon diversity
eliminated
(n=524)
resistant (1st)
(n=128)
resistant (2nd)
(n=50)
static
(n=145)
norm. BC abundance
scaled log2(counts+1)
Avg count day 0
log10(counts+1)
B-ALL
day 4
B-ALL + NK
day 4
B-ALL + NK
day 14

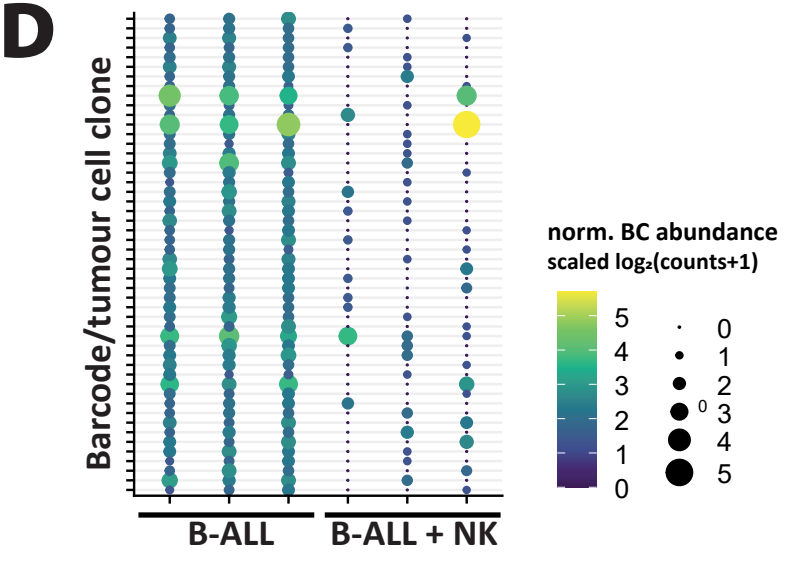
D
Barcode/tumour cell clone
B-ALL
B-ALL + NK
norm. BC abundance
scaled log2(counts+1)

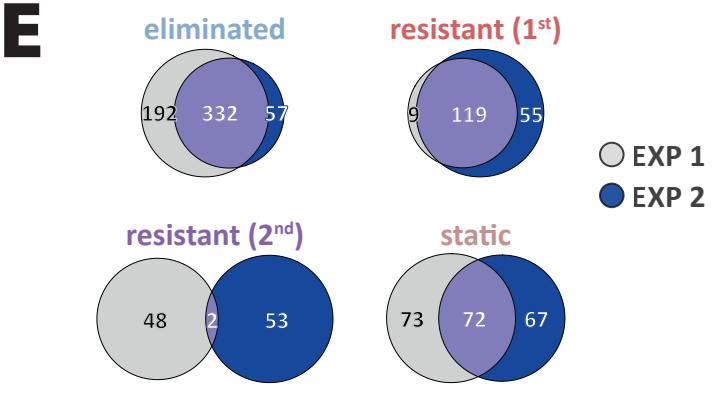
E
eliminated
192
332
57
resistant (1st)
9
119
55
resistant (2nd)
48
2
53
static
73
72
67
EXP 1
EXP 2

Figure 3

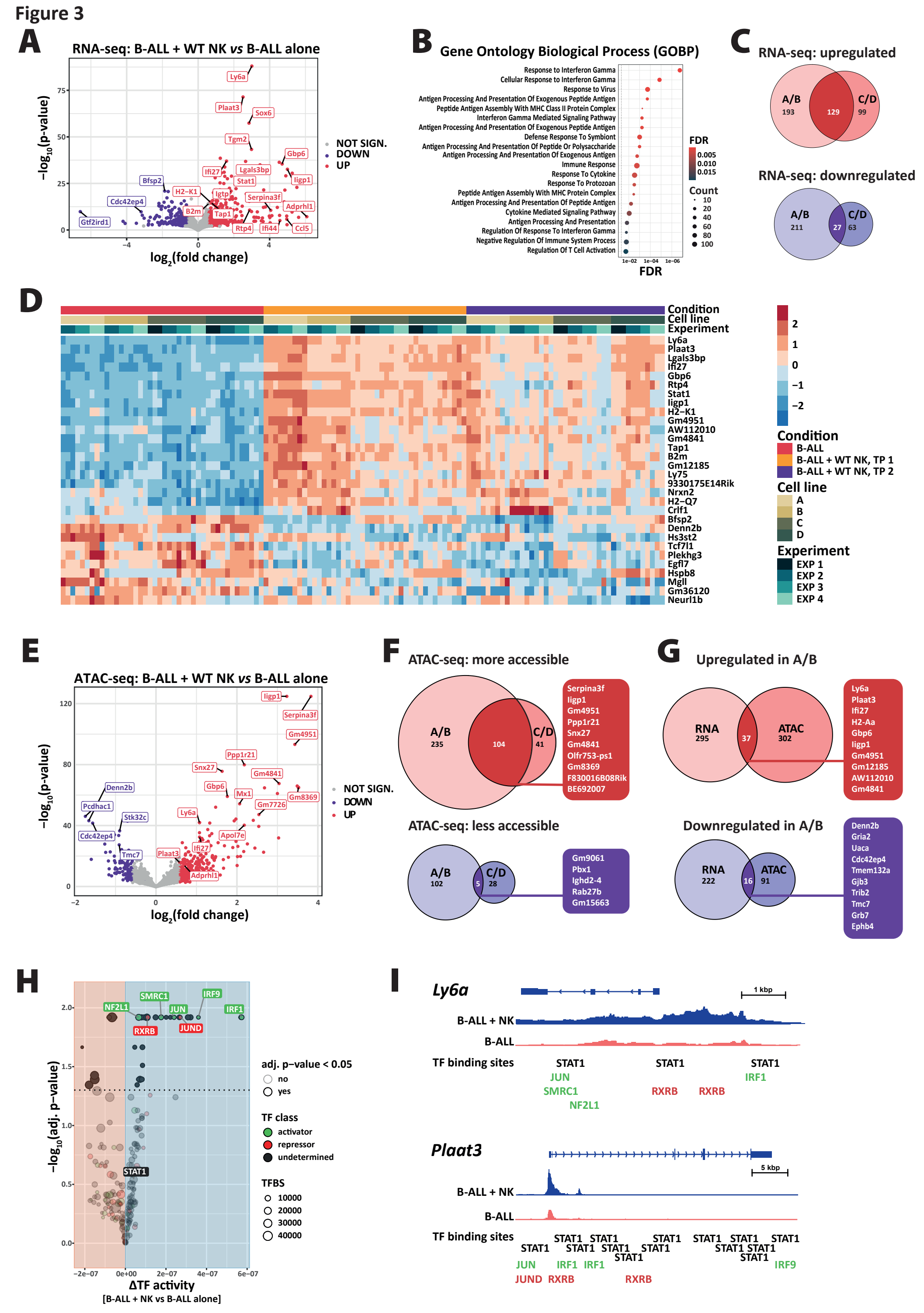
A
RNA-seq: B-ALL + WT NK vs B-ALL alone
−log10(p-value)
log2(fold change)
NOT SIGN.
DOWN
UP
Ly6a
Plaat3
Sox6
Tgm2
Gbp6
Ifi27
Lgals3bp
Stat1
Iigp1
Bfsp2
H2−K1
Igtp
Serpina3f
Cdc42ep4
B2m
Tap1
Adprhl1
Gtf2ird1
Rtp4
Ifi44
Ccl5
B
Gene Ontology Biological Process (GOBP)
Response to Interferon Gamma
Cellular Response to Interferon Gamma
Response to Virus
Antigen Processing And Presentation Of Exogenous Peptide Antigen
Peptide Antigen Assembly With MHC Class II Protein Complex
Interferon Gamma Mediated Signaling Pathway
Antigen Processing And Presentation Of Exogenous Peptide Antigen
Defense Response To Symbiont
Antigen Processing And Presentation Of Peptide Or Polysaccharide
Antigen Processing And Presentation Of Exogenous Antigen
Immune Response
Response To Cytokine
Response To Protozoan
Peptide Antigen Assembly With MHC Protein Complex
Antigen Processing And Presentation Of Peptide Antigen
Cytokine Mediated Signaling Pathway
Antigen Processing And Presentation
Regulation Of Response To Interferon Gamma
Negative Regulation Of Immune System Process
Regulation Of T Cell Activation
FDR
Count
C
RNA-seq: upregulated
A/B 193
129
C/D 99
RNA-seq: downregulated
A/B 211
27
C/D 63
D
Condition
Cell line
Experiment
Ly6a
Plaat3
Lgals3bp
Ifi27
Gbp6
Rtp4
Stat1
Iigp1
H2−K1
Gm4951
AW112010
Gm4841
Tap1
B2m
Gm12185
Ly75
9330175E14Rik
Nrxn2
H2−Q7
Crlf1
Bfsp2
Denn2b
Hs3st2
Tcf7l1
Plekhg3
Egfl7
Hspb8
Mgll
Gm36120
Neurl1b
Condition
B-ALL
B-ALL + WT NK, TP 1
B-ALL + WT NK, TP 2
Cell line
A
B
C
D
Experiment
EXP 1
EXP 2
EXP 3
EXP 4
E
ATAC-seq: B-ALL + WT NK vs B-ALL alone
−log10(p-value)
log2(fold change)
NOT SIGN.
DOWN
UP
Iigp1
Serpina3f
Gm4951
Ppp1r21
Snx27
Gm4841
Gbp6
Mx1
Gm8369
Gm7726
Denn2b
Pcdhac1
Stk32c
Ly6a
Cdc42ep4
Apol7e
Tmc7
Plaat3
Ifi27
Adprhl1
F
ATAC-seq: more accessible
A/B 235
104
C/D 41
Serpina3f
Iigp1
Gm4951
Ppp1r21
Snx27
Gm4841
Olfr753-ps1
Gm8369
F830016B08Rik
BE692007
ATAC-seq: less accessible
A/B 102
5
C/D 28
Gm9061
Pbx1
Ighd2-4
Rab27b
Gm15663
G
Upregulated in A/B
RNA 295
37
ATAC 302
Ly6a
Plaat3
Ifi27
H2-Aa
Gbp6
Iigp1
Gm4951
Gm12185
AW112010
Gm4841
Downregulated in A/B
RNA 222
16
ATAC 91
Denn2b
Gria2
Uaca
Cdc42ep4
Tmem132a
Gjb3
Trib2
Tmc7
Grb7
Ephb4
H
−log10(adj. p−value)
ΔTF activity
[B-ALL + NK vs B-ALL alone]
NF2L1
SMRC1
JUN
IRF9
IRF1
RXRB
JUND
STAT1
adj. p−value < 0.05
no
yes
TF class
activator
repressor
undetermined
TFBS
10000
20000
30000
40000
I
Ly6a
1 kbp
B-ALL + NK
B-ALL
TF binding sites
STAT1
JUN
SMRC1
NF2L1
RXRB
IRF1
Plaat3
5 kbp
IRF9

Figure 4

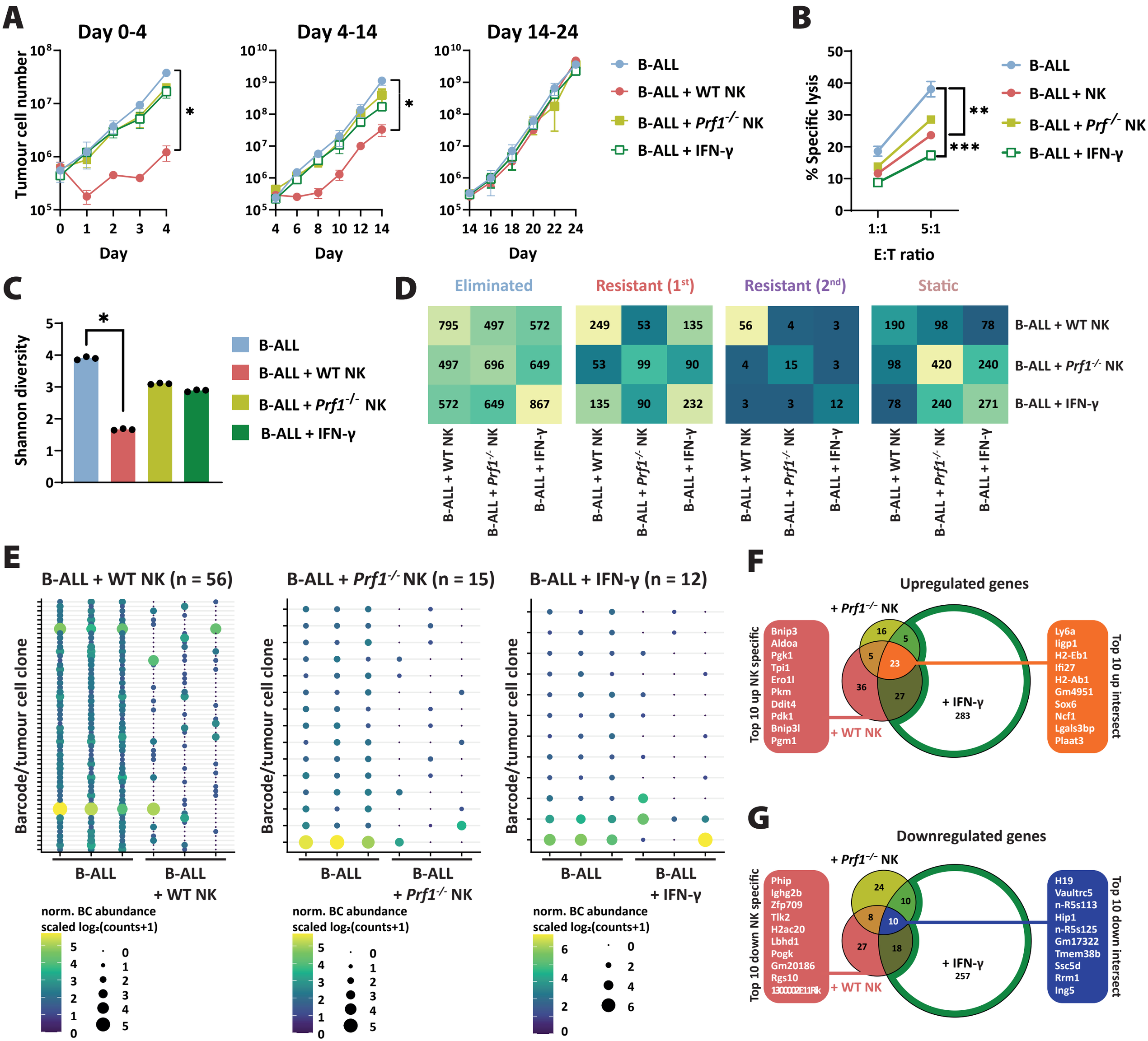
A
Day 0-4
Day 4-14
Day 14-24
Tumour cell number
Day
B-ALL
B-ALL + WT NK
B-ALL + Prf1-/- NK
B-ALL + IFN-γ
B
% Specific lysis
E:T ratio
1:1
5:1
C
Shannon diversity
D
Eliminated
Resistant (1st)
Resistant (2nd)
Static
795 497 572
497 696 649
572 649 867
249 53 135
53 99 90
135 90 232
56 4 3
4 15 3
3 3 12
190 98 78
98 420 240
78 240 271
E
B-ALL + WT NK (n = 56)
B-ALL + Prf1-/- NK (n = 15)
B-ALL + IFN-γ (n = 12)
Barcode/tumour cell clone
B-ALL
B-ALL + WT NK
B-ALL + Prf1-/- NK
B-ALL + IFN-γ
norm. BC abundance
scaled log2(counts+1)
F
Upregulated genes
+ Prf1-/- NK
+ WT NK
+ IFN-γ
283
Top 10 up NK specific
Bnip3
Aldoa
Pgk1
Tpi1
Ero1l
Pkm
Ddit4
Pdk1
Bnip3l
Pgm1
Top 10 up intersect
Ly6a
Iigp1
H2-Eb1
Ifi27
H2-Ab1
Gm4951
Sox6
Ncf1
Lgals3bp
Plaat3
G
Downregulated genes
+ Prf1-/- NK
+ WT NK
+ IFN-γ
257
Top 10 down NK specific
Phip
Ighg2b
Zfp709
Tlk2
H2ac20
Lbhd1
Pogk
Gm20186
Rgs10
1300002E11Rik
Top 10 down intersect
H19
Vaultrc5
n-R5s113
Hip1
n-R5s125
Gm17322
Tmem38b
Ssc5d
Rrm1
Ing5

Figure 5

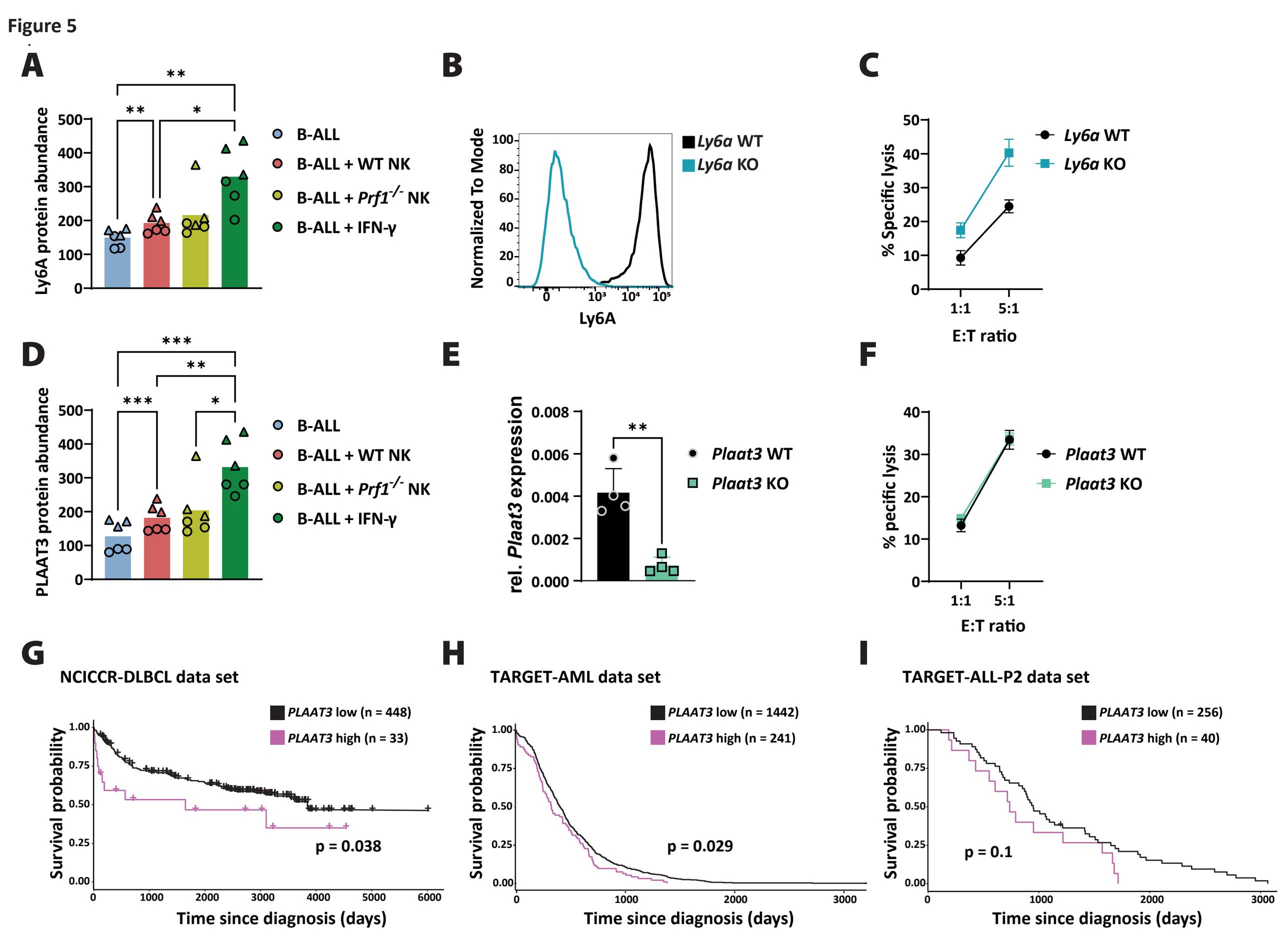
A
Ly6A protein abundance
B-ALL
B-ALL + WT NK
B-ALL + Prf1-/- NK
B-ALL + IFN-γ
B
Normalized To Mode
Ly6A
Ly6a WT
Ly6a KO
C
% Specific lysis
E:T ratio
Ly6a WT
Ly6a KO
D
PLAAT3 protein abundance
B-ALL
B-ALL + WT NK
B-ALL + Prf1-/- NK
B-ALL + IFN-γ
E
rel. Plaat3 expression
Plaat3 WT
Plaat3 KO
F
% pecific lysis
E:T ratio
Plaat3 WT
Plaat3 KO
G
NCICCR-DLBCL data set
PLAAT3 low (n = 448)
PLAAT3 high (n = 33)
p = 0.038
Survival probability
Time since diagnosis (days)
H
TARGET-AML data set
PLAAT3 low (n = 1442)
PLAAT3 high (n = 241)
p = 0.029
Survival probability
Time since diagnosis (days)
I
TARGET-ALL-P2 data set
PLAAT3 low (n = 256)
PLAAT3 high (n = 40)
p = 0.1
Survival probability
Time since diagnosis (days)